University of Chicago
Physics 575
Accelerator Physics and Technology of Linear Colliders

Chapter 7

Superconducting RF

Winter 2002

Lutz Lilje
DESY -MPY-

Peter Schmüser
Universität Hamburg

For the help in preparing this lecture I would thank Prof. Peter Schmüser. The work of all the colleagues in the TESLA collaboration making this lecture possible is gratefully acknowledged.

Contents

Introduction

Superconducting radiofrequency resonators for particle acceleration have become a standard component for particle accelerators. Particle bunches with high currents are accelerated with high efficiency as the power dissipated in the cavity walls is very low. The available radiofrequency power is nearly completely converted to particle energy. This high efficiency of superconducting accelerating cavities is used in continuous particle beam accelerators as CEBAF as well as in high current applications as in CESR.

The high quality factor and the small dissipation in the wall allow for cavities with large volume as accelerating structures and low frequencies as compared to high gradient normalconducting copper structures. The optimum accelerating gradient for a continuous wave operation for superconducting cavities is between 10 - 15 MV/m. For gradients of more than 20 MV/m it is necessary to go to a pulsed operation to reduce the cryogenic losses which scale with the square of the accelerating gradient. Still, long pulses of about a millisecond with low radiofrequency (RF) peak power are possible. This has to be compared with very short pulses in the order of microseconds for copper accelerating structures. The effect of wakefields which can influence the beam quality is also reduced by the large apertures of low frequency cavities. The alignment tolerances for superconducting structures are more relaxed than for the higher frequency normalconducting cavities. A low beam emittance can be preserved in a linac. This makes a superconducting linac a very good driver for a free electron laser.

The lecture will describe the features of superconducting cavities in the context of the TESLA[1] project. It has to be mentioned that today there exist a lot of rather new projects (some of which are only in their design stage) which rely on superconducting cavities not only for electrons[2] but also for other particles like protons (SNS, LHC) and ions (RIA). The reason for this is that niobium superconducting cavities are well enough understood to achieve magnetic surface fields of around 100 mT reliably. The TESLA-Collaboration aims for the realization of a linear collider in the TeV energy range. In this project particle beams of electrons and positrons are accelerated with superconducting cavities made from niobium to energies of 250 GeV and brought to head-on collision. An X-ray free electron laser is integrated in the design of the accelerator. A pulsed high frequency field at 1.3 GHz is used for particle acceleration.

The first chapter will deal with pulsed resonant cavities as used in particle accelerators. In the second chapter, the focus will be on the superconductivity related issues of critical magnetic fields and RF surface resistance. The

[1] TESLA stands for "TeV Energy Superconducting Linear Accelerator". Details in [Brinkmann et al. 1997] and [Brinkmann et al. 2001].

[2] These are usually FELs (SCA, JLab, BESSY), synchrotron light sources like Soleil but also storage rings for particle physics like KEK-B or CESR.

typical limitations of bulk niobium cavities are reviewed. In the third chapter the TESLA cavities will serve as an example on how to design and built superconducting cavities. The typical performance of state-of-the-art cavities will be presented and an outlook what might be achieved in future in superconducting niobium resonators. Finally, some of the necessary technical auxiliary systems like cryostats, couplers and RF control will be discussed in the fourth chapter.

1 Basics of radiofrequency cavities

In this chapter the basic properties of radiofrequency cavities are reviewed.[3] The surface resistance and its dependence on temperature and surface magnetic and electric field will be introduced. Then the methods used within the TESLA collaboration to maximize the accelerating gradients and the results achieved to date are presented.

1.1 Accelerating cavities - Figures of merit

Accelerating cavities are used to increase the energy of a charged particle beam[4]. Obviously, the energy gain per unit length is therefore an important parameter of accelerating cavities. This is conveniently derived from the accelerating voltage a particle with charge e experiences while traversing the cavity:

$$V_{acc} = \left| \frac{1}{e} \times \text{energy gain during transit} \right| \tag{1}$$

For particles travelling with the velocity of light c on the symmetry axis in z-direction ($\rho = 0$) and a accelerating mode with eigenfrequency ω this gives:

$$V_{acc} = \left| \int_0^d E_z(z)\ e^{i\omega z/c}\ \mathrm{d}z \right| \tag{2}$$

The accelerating field is

$$E_{acc} = \frac{V_{acc}}{d} \tag{3}$$

To sustain the radiofrequency fields in the cavity, an alternating current is flowing in the cavity walls. This current dissipates power in the wall as it

[3] A good introduction into superconducting cavities is given in [Padamsee et al. 1998]. Short review articles are also available [Padamsee 2001, Aune et al. 2000]

[4] There are a few applications where resonant cavities are used to decelerate or deflect particle beams.

experiences a surface resistance[5]. One can look at the power P_{diss} which is dissipated in the cavity to define the global surface resistance R_{surf}:

$$P_{diss} = \frac{1}{2}\oint_A R_{surf} H_{surf}^2 \mathrm{d}A \tag{4}$$

$$= \frac{1}{2} R_{surf} \oint_A H_{surf}^2 \mathrm{d}A \tag{5}$$

Here H_{surf} denotes the magnetic field amplitude. Usually, one measures the quality factor[6] Q_0:

$$Q_0 = \frac{\omega W}{P_{diss}}, \tag{6}$$

where

$$W = \frac{1}{2}\mu_0 \int_V H^2 \mathrm{d}V \tag{7}$$

is the energy stored in the electromagnetic field in the cavity. R_{surf} is an integral surface resistance for the cavity. The surface resistance and the quality factor are related via the geometrical constant G which depends only on the geometry of a cavity and field distribution of the excited mode, but not on the resistivity of the material:

$$G = \frac{\omega\mu_0 \int_V H^2 \mathrm{d}V}{\oint_A H^2 \mathrm{d}A} \tag{8}$$

This gives

$$Q_0 = \frac{\omega\mu_0 \oint_V H^2 \mathrm{d}V}{R_{surf} \oint_A H^2 \mathrm{d}A} = \frac{G}{R_{surf}} \tag{9}$$

For the typical elliptical shape of superconducting cavities $G = 270\ \Omega$. For a nine-cell TESLA cavity the quality factor is typically $Q_0 = 1.2 \cdot 10^{10}$ at $T = 2$ K corresponding to a surface resistance of $R_{surf} = 10\ \mathrm{n}\Omega$.

One can see that the efficiency with which a particle beam can be accelerated in an radiofrequency cavity depends on the surface resistance. The smaller the resistance i.e. the lower the power dissipated in the walls, the higher the radiofrequency power available for the particle beam. This is the fundamental advantage of superconducting cavities as their surface resistance is much lower and outweighs the power needed to cool the cavities to liquid helium temperatures. A nine-cell cavity dissipates about 100 W at 25 MV/m with a $Q_0 = 5 \cdot 10^9$. In the pulsed operation of TESLA with a duty cycle of 1% this is only 1 W of radiofrequency power, whereas 200 kW are available for the beam as shown in table 5.

[5]This also the case for a superconductor where alternating fields give rise to the surface resistance for temperatures $T > 0$ K. More details can be found in section 2.3.1.

[6]The quality factor can also be defined as $Q_0 = f/\Delta f$ where f is the resonance frequency and Δf the full width at half height of the resonance curve in an unloaded cavity.

1.1.1 Example: The Pillbox cavity

Field pattern The simplest model of an accelerating cavity is a hollow cylinder which is often called pill box. When the beam pipes are neglected the field pattern inside the resonator and all relevant cavity parameters can be calculated analytically. For particle acceleration we need a longitudinal electric field on the axis, hence we look for TM (transverse magnetic) eigenmodes of the cylindrical resonator. We use cylindrical coordinates (r, θ, z) where z denotes the beam direction (cavity axis), $r = \sqrt{x^2 + y^2}$ and θ the azimuthal angle. We search for an eigenmode with cylindrical symmetry (independence of θ) and with longitudinal electric and azimuthal magnetic field. The wave equation for the electric field reads

$$\frac{\partial^2 E_z}{\partial r^2} + \frac{1}{r}\frac{\partial E_z}{\partial r} = \frac{1}{c^2}\frac{\partial^2 E_z}{\partial t^2}\,. \tag{10}$$

For a harmonic time dependence $E_z(r)\cos(\omega t)$ and with the new variable $u = r\omega/c$ one obtains

$$\frac{\partial^2 E_z}{\partial u^2} + \frac{1}{u}\frac{\partial E_z}{\partial u} + E_z(u) = 0\,. \tag{11}$$

This is the Bessel equation of zero order with the solution $J_0(u)$. Hence the radial dependence of the electric field is

$$E_z(r) = E_0 J_0(\frac{\omega r}{c})\,. \tag{12}$$

For a perfectly conducting cylinder of radius R the longitudinal electric field must vanish at $r = R$, so $J_0(\omega R/c) = 0$. The first zero of $J_0(u)$ is at $u = 2.405$. This defines the frequency of the eigenmode (we call it the fundamental mode in the following):

$$f_0 = \frac{2.405c}{2\pi R}\,, \quad \omega_0 = \frac{2.405c}{R}\ . \tag{13}$$

In a cylindrical cavity the frequency does not depend on the length. The magnetic field can be computed from the equation

$$\frac{\partial E_z}{\partial r} = \frac{\partial B_\theta}{\partial t}\,. \tag{14}$$

Hence we obtain for the fundamental TM mode

$$E_z(r,t) = E_0 J_0(\frac{\omega_0 r}{c})\cos(\omega_0 t)\,, \quad H_\theta(r,t) = -\frac{E_0}{\mu_0 c} J_1(\frac{\omega_0 r}{c})\sin(\omega t)\ . \tag{15}$$

Electric and magnetic field are 90° out of phase. The azimuthal magnetic field vanishes on the axis and assumes its maximum close to the cavity wall. A field profile is shown in figure 1.

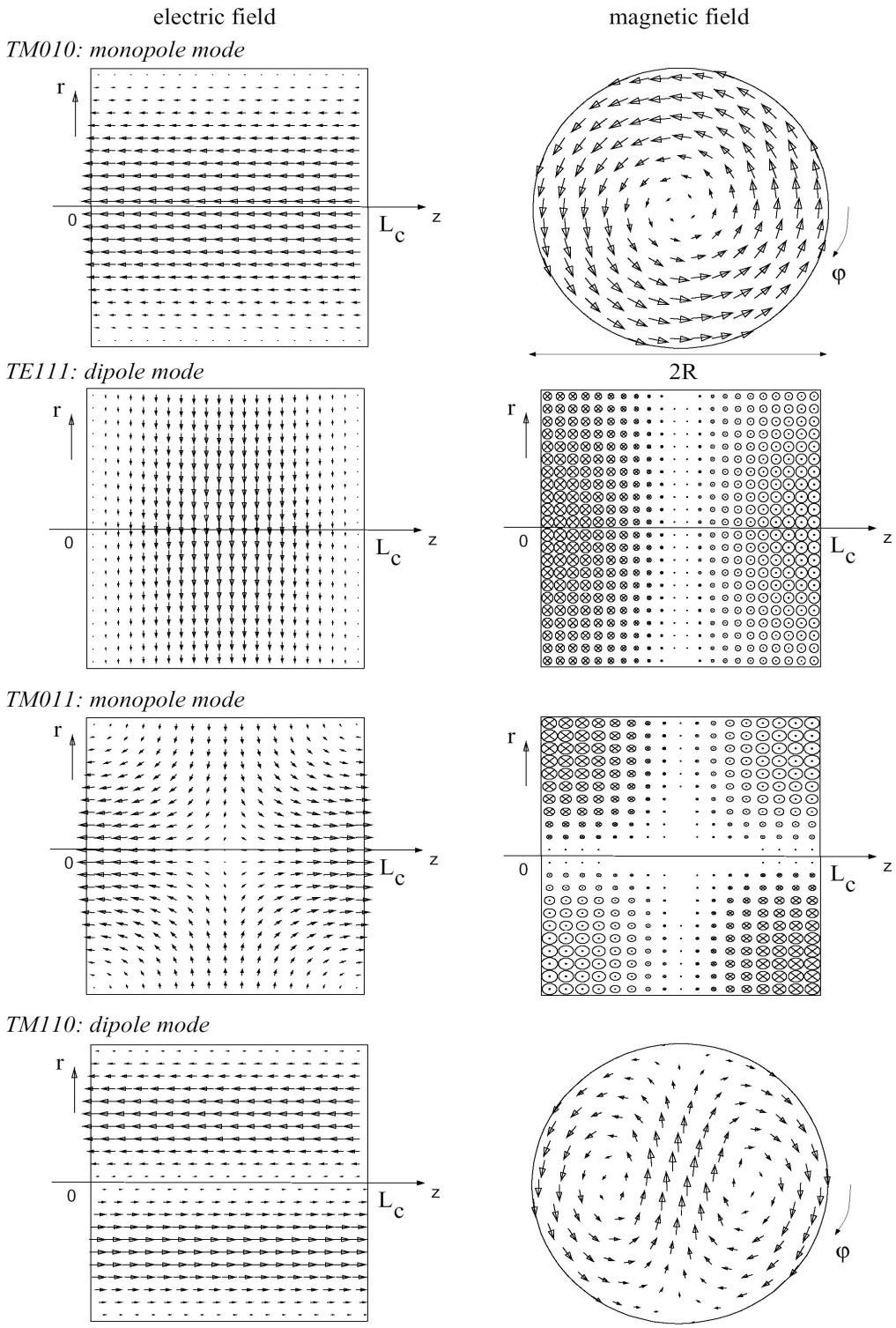

Figure 1: Electric and magnetic field in a pillbox cavity for several resonant modes (Courtesy of M. Liepe).

Stored energy The electromagnetic field energy is computed by integrating the energy density $(\varepsilon_0/2)E^2$ (at time $t = 0$) over the volume of the cavity. This yields

$$U = \frac{\varepsilon_0}{2}\, 2\pi\ell E_0^2 \int_0^R J_0^2(\frac{\omega_0 r}{c}) r dr = \frac{\varepsilon_0}{2}\, 2\pi\ell E_0^2 \left(\frac{c}{\omega_0}\right)^2 \int_0^a J_0^2(u) u du \qquad (16)$$

where $a = 2.405$ is the first zero of J_0. Using the relation $\int_0^a J_0^2(u)udu = 0.5(aJ_1(a))^2$ we get for the energy stored in the cavity

$$U = \frac{\varepsilon_0}{2}\, E_0^2(\pi R^2\ell)(J_1(2.405))^2\,. \qquad (17)$$

Here $(\pi R^2\ell)$ is the volume of the cavity and $J_1(2.405) = 0.52$.

Power dissipation in the cavity Here we consider a cavity made from a normal metal. e.g. copper. The rf electric field causes basically no losses since its tangential component vanishes at the cavity wall while the azimuthal magnetic field penetrates into the wall with exponential attenuation and induces currents within the skin depth[7]. These alternating currents lead to Ohmic heat generation. The skin depth is given by

$$\delta = \sqrt{\frac{2}{\mu_0\omega\sigma}} \qquad (18)$$

where σ is the conductivity of the metal. For copper at room temperature and a frequency of 1 GHz the skin depth is $\delta = 2\mu$m. Consider now a small surface element. From Ampere's law $\oint \vec{H}\cdot\vec{ds} = I$ follows that the current density in the skin depth is related to the azimuthal magnetic field by $j = H_\theta/\delta$. Then the dissipated power per unit area is

$$\frac{dP_{diss}}{dA} = \frac{1}{2\sigma\delta}\, j^2 = \frac{1}{2} R_{surf} H_\theta^2\,. \qquad (19)$$

Here we have introduced a very important quantity for rf cavities, the *surface resistance*:

$$R_{surf} = \frac{1}{\sigma\delta}\,. \qquad (20)$$

The power density has to be integrated over the whole inner surface of the cavity. This is straightforward for the cylindrical mantle where $H_\theta = \frac{E_0}{\mu_0 c} J_1(\omega_0 R/c)$ is constant. To compute the power dissipation in the circular

[7]For a very careful discussion of the skin effect see J.D. Jackson, Classical Electrodynamics, chapt. .

end plates one has to evaluate the integral $\int_0^a (J_1(u))^2 u du = u^2 (J_1(a))^2/2$. Again $a = 2.405$ is the first zero of J_0. The total dissipated power in the cavity walls is then

$$P_{diss} = R_{surf} \cdot \frac{E_0^2}{2\mu_0^2 c^2} (J_1(2.405))^2 2\pi R\ell(1 + R/\ell) \,. \tag{21}$$

Quality factor The quality factor is an important parameter of a resonating cavity. It is essentially the ratio of stored energy to energy loss per oscillation cycle or, alternativerly, the ratio of resonance frequency f_0 and the full width at half maximum of the resonance curve Δf

$$Q_0 = \omega_0 \cdot \frac{U}{P_{diss}} = \frac{f_0}{\Delta f} \,. \tag{22}$$

Using the formulas (17) and (21) we get the important equation

$$Q_0 = \frac{G}{R_{surf}} \quad \text{with} \quad G = \frac{2.405\mu_0 c}{2(1 + R/\ell)} \tag{23}$$

which states that the quality factor of a cavity is obtained by dividing the so-called "geometry constant" G by the surface resistance. G depends only on the shape of the cavity and not on the material. A typical value is 300 Ω. We want to point out that the quality factor Q_0 defined here is the intrinsic or "unloaded" quality factor of a cavity. If the cavity is connected to an external load resistor by means of a coupler another quality factor (Q_{ext}) has to be introduced to account for the energy extraction through the coupler (see sect. 1.2).

Accelerating field A relativistic particle needs a time c/ℓ to travel through the cavity. During this time the longitudinal electric field changes. The accelerating field is defined as the average field seen by the particle

$$E_{acc} = \frac{1}{\ell} \int_{-\ell/2}^{\ell/2} E_0 \cos(\omega_0 z/c) dz \,, \qquad V_{acc} = E_{acc}\, \ell \,. \tag{24}$$

Choosing a cell length of one half the rf wavelength, $\ell = c/(2f_0)$, we get $E_{acc} = 0.64\, E_0$ for a pill box cavity .

1.2 Coupling of rf power into the cavity

The purpose of an accelerating cavity is to transfer radio frequency power to the particle beam. The rf cavities in a storage ring are necessarily operated

in the *continuous wave* (cw) mode while in a high energy linear accelerator usually a pulsed operation is needed. In a normal conducting linac like SLAC the rf pulses must be quite short, in the order of microseconds, to prevent overheating of the copper structures, in the superconducting TESLA the pulse duration may be a millisecond. Thereby the heat load on the refrigeration system is kept within tolerable limits. In the following we consider first the cw mode.

Equivalent circuit diagram for a cavity coupled to an rf power source We represent the sc cavity by an LCR circuit (Fig. 2) where the parallel resistor R_0, often called the *shunt impedance*, is very large ($> 10^{12}\Omega$ at $T = 2$ K). The incorporation of the rf power source into this circuit diagram requires some care because the rf wave is guided to the cavity through a transmission line, and reflections may occur at the input to the cavity.

The standard rf power sources for sc cavities used for particle acceleration are klystrons with a power rating of typically a MW while for cavity tests without beam solid state amplifiers of 100-1000 W can be used. The rf wave is transported to the cavity through a transmission line (waveguide at high power, coaxial cable at low power) and coupled into the resonator by means of an input coupler. This can be a waveguide coupler or a coaxial coupler. The simplest input coupler, which is commonly used in the acceptance test of an sc cavity, is a coaxial antenna in the beam pipe section of the cavity (see Fig. 32). The radius of the pipe is chosen such that its cut-off frequency is above the resonant frequency of the cavity. Hence the standing wave in the resonator is exponentially attenuated in the pipe. This means that the electric field amplitude at the tip of the coaxial antenna depends strongly on the antenna position and can be varied by several orders of magnitude when the antenna is moved longitudinally be just a few cm. Effectively, the input coupler acts as a transformer with a variable transformation ratio $1 : n$ (usually $n \gg 1$).

It often happens that the rf wave is partly reflected at the input coupler and travels back to the rf source. Klystrons but also amplifiers may be destroyed by reflected rf waves. For that reason a *circulator* is introduced into the wave guide section between klystron and cavity, see Fig. 2. The circulator has the following property: an rf wave entering at port 1 leaves the circulator at port 2, a wave entering at port 2 leaves at port 3. Port 3 is terminated with a load resistor having the characteristic impedance Z_1 of the transmission line. The wave reflected at the cavity input is thus guided into the load resistor at port 3 and completely absorbed there. Seen from the klystron, the wave guide is therefore always properly terminated, see the

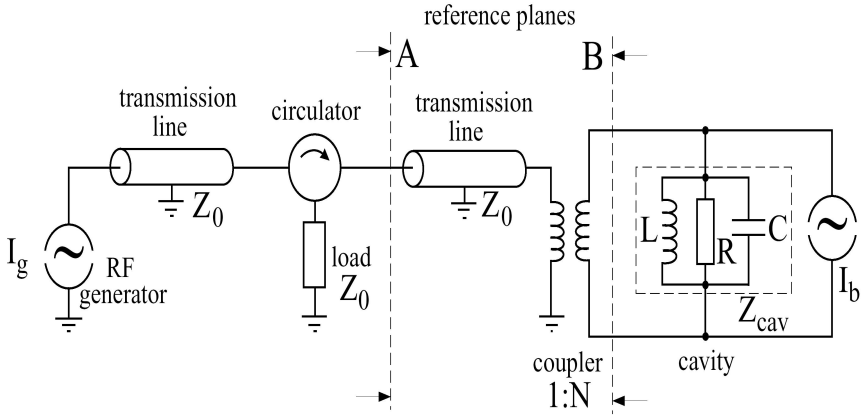

Figure 2: Equivalent circuit for generator-cavity-system (Overview).

simplified circuit diagram of Fig. 3a). A simplified circuit diagram which does not contain any transmission line components can also be drawn for the cavity side, see Fig. 3b. The wave guide with its termination Z_1 at port 3 of the circulator is transformed into the circuit as a parallel external resistance $R_{ext} = n^2 \cdot Z_1$. The klystron is represented as an alternating current source.

The intrinsic quality factor of the cavity reads in terms of the lumped-circuit components

$$Q_0 = \frac{R_0}{\omega_0 L} \quad \text{with} \quad \omega_0 = 1/\sqrt{LC}\,. \tag{25}$$

The external load leads to an additional damping of a free oscillation in the LC circuit. The corresponding quality factor is called the external Q of the cavity

$$Q_{ext} = \frac{R_{ext}}{\omega_0 L} \quad \text{with} \quad \omega_0 = 1/\sqrt{LC}\,. \tag{26}$$

The parallel resistors R_0 and R_{ext} can be replaced by $R_{load} = (1/R_0 + 1/R_{ext})^{-1}$ which defines the *loaded qualitiy factor*

$$Q_{load} = \frac{R_{load}}{\omega_0 L}\,, \quad \frac{1}{Q_{load}} = \frac{1}{Q_0} + \frac{1}{Q_{ext}}\,. \tag{27}$$

Now we consider a driven oscillation of the circuit by applying a harmonic current. For simplicity we assume that the generator frequency coincides with the cavity eigenfrequeny. Then Kirchhoff's rule yields

$$C\,\frac{dV}{dt} + \frac{V}{R_{load}} + \frac{1}{L}\int V\,dt = i_g \cos(\omega_0 t)\,. \tag{28}$$

a) left side of reference plane A:

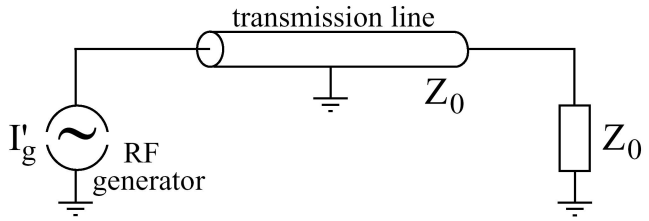

b) right side of reference plane A:

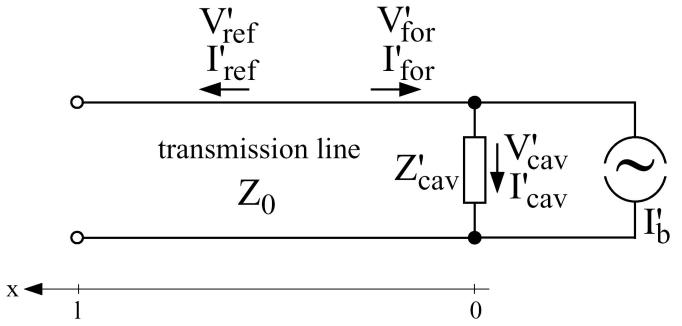

c) right side of reference plane B:

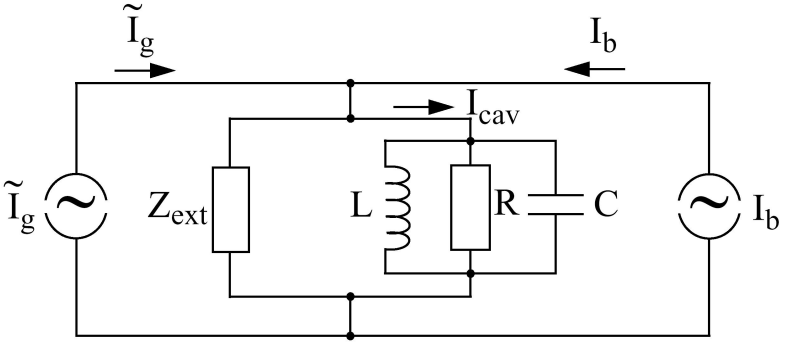

Figure 3: Equivalent circuit (seperated planes).

Taking the derivate with respect to time we get the equation of a driven harmonic oscillator

$$\frac{d^2V}{dt^2} + \frac{\omega_0}{Q_{load}} \cdot \frac{dV}{dt} + \omega_0^2 V = -\frac{i_g \omega_0}{C} \sin(\omega_0 t) \; . \tag{29}$$

The stationary solution is

$$V(t) = i_g R_{load} \cos(\omega_0 t) \; . \tag{30}$$

When the current is switched off we get a damped free oscillation with the damping time constant

$$\tau = \frac{2Q_{load}}{\omega_0} \; . \tag{31}$$

The voltage transients in pulsed operation are discussed below.

Test of cavity without beam The ideal condition is that the rf generator frequency equals the cavity eigenfrequency, $\omega_g = \omega_0$, and that no power is reflected at the input coupler. This is realized if the transformed cavity impedance is equal to the characteristic impedance of the wave guide:

$$Z_{cav}/n^2 = R_0/n^2 = Z_1 \; . \tag{32}$$

Note that for $\omega_g = \omega_0$ the impedance of the LCR circuit is purely real and given by R_0. Under these conditions $Q_{load} = Q_0/2$, and from the time decay of the oscillation after switching off the rf generator one can easily determine the intrinsic quality factor Q_0. The generator power is fully transmitted into the cavity and dissipated in the walls, so $P_g = P_{diss}$. Measuring P_g with a power meter allows one then to compute the stored energy $U = Q_0 P_{diss}/\omega_0$ and the accelerating field in the cavity (in case of a pill box cavity with the help of Eq. (17), for other cavity shapes by means of numerical codes).

It is convention to define a coupling parameter β_c by

$$\beta_c = \frac{R_0}{n^2 Z_1} \; . \tag{33}$$

Proper termination of the transmission line means $\beta_c = 1$. If this is not the case, the incident rf generator power P_g will be partly reflected at the input coupler, partly transmitted through the coupler and dissipated in the cavity walls:

$$P_{ref} = \frac{(\beta_c - 1)^2}{(\beta_c + 1)^2} P_g \; , \qquad P_{trans} = P_{diss} = \frac{4\beta_c}{(\beta_c + 1)^2} P_g \; . \tag{34}$$

For unity coupling, $\beta_c = 1$, the klystron power P_g is fully transmitted and dissipated in the resistance R_0. In the simplified circuit diagram of

Fig. 3b, however, the generator current flows not only through the cavity shunt impedance R_0 but also through the external resistance R_{ext}. Hence the generator current i_g is a fictitious quantity and different from the real klystron current. It can be computed for arbitrary β_c from the generator power in the following way: According to Fig. 3b the power dissipated in R_0 is $i_g^2 R_0/(2(\beta_c+1)^2$. Comparing with Eq. (34) we obtain

$$i_g = 2\sqrt{\frac{2\beta_c P_g}{R_0}} \tag{35}$$

which means that in matched condition ($\beta_c = 1$ and $R_{ext} = R_0$) the fictitious source current is twice the klystron current.

1.3 Acceleration of a bunched beam

A radio frequency cavity cannot transfer energy to a continuous beam because half of the time the field is decelerating. On the contrary, the particles must be grouped in short bunches which are synchronized with the rf wave to pass the cavity always at the desired rf phase. Respresenting the accelerating electric field by $E_z(t) = E_0 \cos(\omega_g t)$, the nominal phase for a relativistic beam ($v \approx c$) must be chosen on the falling slope of the rf wave ($0 < \phi_0 < \pi/2$) in order to achieve longitudinal focusing in a circular accelerator, while in a linac the particles are usually accelerated "on crest" ($\phi_0 = 0$). A bunch train consists of many equally spaced bunches whose repetition time T_b is an integer multiple of the rf period, $T_b = h\,T_g$ (h is called the harmonic number). The bunch length is much smaller, $\Delta t_b \ll T_g$. In good approximation one can treat the bunch train as a periodic sequence of δ pulses whose Fourier component at the rf frequency ($\omega_g = h\,\omega_{rep}$) interacts with the rf wave in the cavity. This Fourier component is twice the dc component I_0 of the beam. In the lumped-circuit diagram of figure 2 the beam is represented by a current whose direction is chosen opposite to the generator current because the beam extracts energy from the cavity. The generator and beam currents are respectively

$$\tilde{i}_g \exp(i\omega_g t)\,, \qquad \tilde{i}_b \exp(i\omega_g t) \tag{36}$$

where $\tilde{i}_g$ and $\tilde{i}_b$ are complex phasors with $|\tilde{i}_g| = i_g$ and $|\tilde{i}_b| = 2\,I_0$. We consider here only the case that the generator frequeny and cavity eigenfrequency are equal $\omega_g = \omega_0$ and that the buches are accelerated "on crest". The generator-induced and beam-induced voltages in the LCR circuit are

$$\tilde{V}_g = \tilde{i}_g \frac{R_0}{\beta_c + 1}\,, \qquad \tilde{V}_b = \tilde{i}_b \frac{R_0}{\beta_c + 1} \tag{37}$$

The accelerating voltage is the vectorial sum of these two voltages

$$\tilde{V}_{acc} = \tilde{V}_g + \tilde{V}_b \; . \tag{38}$$

It is this quantity which changes the particle energy. For on-crest acceleration, the generator- and beam-induced voltages point in opposite direction, see Fig. 4, and the net acceleration voltage is $V_{acc} = V_g - V_b$. Using Eq. (35) to express the fictive generator current i_g by the generator power P_g (i.e. the klystron power) and replacing the Fourier component of the beam current at ω_g by the dc component ($i_b = 2I_0$) we get the following expression for the cavity voltage

$$V_{acc} = \frac{2\sqrt{2\beta_c P_g R_0}}{\beta_c + 1} \cdot (1 - K/\sqrt{\beta_c}) \quad \text{with} \qquad K = I_0 \sqrt{\frac{R_0}{2P_g}} \; . \tag{39}$$

The dimensionless quantity K is called the beam loading parameter. The power transferred to the beam is

$$P_b = \frac{i_b V_{acc}}{2} = I_0 \, V_{acc} \; . \tag{40}$$

The efficiency of energy transfer from generator to beam is

$$\eta_g = \frac{P_b}{P_g} = \frac{4K\sqrt{\beta_c}}{\beta_c + 1} \, (1 - K/\sqrt{\beta_c}) \; . \tag{41}$$

Finally, the power reflected at the input coupler is given by

$$P_{ref} = P_g - P_b - P_{diss} = \frac{(\beta_c - 1 - 2K\sqrt{\beta_c})^2}{(\beta_c + 1)^2} \cdot P_g \; . \tag{42}$$

Without beam ($I_0 = 0$ and $K = 0$) we recover the condition $\beta_c = 1$ for zero power reflection at the input coupler. With beam, however, the coupling parameter of a superconducting cavity must be chosen much larger than 1 in order to achieve zero reflection. As an example we consider the 9-cell TESLA cavitiy at 2 Kelvin. The intrinsic quality factor at $E_{acc} = 25$ MV/m is $Q_0 \approx 10^{10}$. The length is about 1 m, so the cavity voltage is $V_{acc} = 25$ MV. For a bunched beam with dc current $I_0 = 8$ mA the generator power is $P_g = 200$ kW. This yields a beam loading parameter $K = 28.8$ and a coupling parameter $\beta_c = 3330$. The external quality factor $Q_{ext} = 3 \cdot 10^6$ is almost 4 orders of magnitude smaller than Q_0. The efficiency of energy transfer from generator to beam is very large, $\eta_g = 99.97\%$. Hence almost the full generator power of 200 kW is transferred to the beam and only 60 W are dissipated in the cavity walls. In a copper cavity, typically 50% of the generator power is wasted in heating the walls.

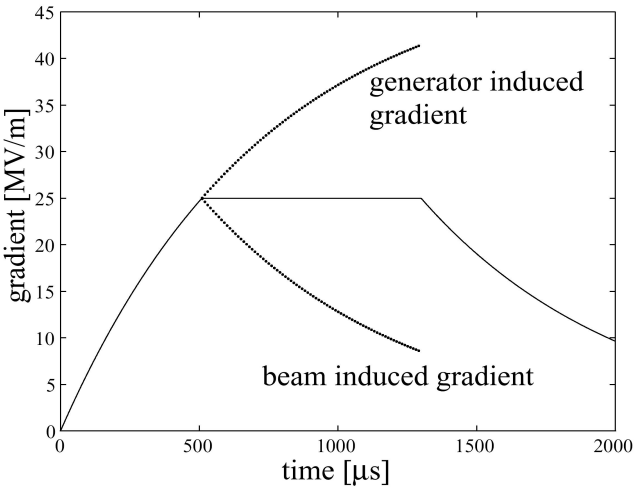

Figure 4: Cavity voltage for the standing wave TESLA cavities during one RF pulse.

Table 1: Typical parameters of the 1.3 GHz superconducting 9-cell TESLA cavity.

beamcurrent	Q_{ext}	β_c	τ	P_g	P_{diss}
$I_0 = 0$	10^{10}	1	1 [s]	60 W2	60 W
$I_0 = 8$mA	$3 \cdot 10^6$	3300	500μs	200 kW2	60 W

1.4 Pulsed cavity operation

Although the dissipated power in a sc cavity amounts to only $0.02 - 0.3\%$ of the generator power, a heat deposition of about 50 W per meter length is far too big for the cryogenic system of a long linac. To reduce the heat load the cavites are operated in pulsed mode with a duty cycle of less than 1%. In pulsed operation the rf power is switched on at time $t = 0$, kept constant during the interval $0 \leq t \leq T_{end}$ and then switched off. The generator-induced voltage rises from zero and approaches its maximum value $V_{max} = i_g \frac{R_0}{\beta_c+1}$ exponentially with the cavity time constant $\tau = 2Q_{load}/\omega_0$

$$V_g(t) = V_{max}(1 - \exp(t/\tau)) \,, \qquad V_{max} = i_g \frac{R_0}{\beta_c + 1} \,. \tag{43}$$

The injection of the bunched beam starts at a time $T_{inj} = \ln 2\tau$ when the generator-induced voltage has reached $V_{max}/2$ (see Fig. 5). Each bunch of charge q_0 acts as a δ-like current pulse, inducing the voltage $v_b = -q_0/(2C)$. For a periodic train of bunches these voltages add up and yield the voltage $V_b(t)$ shown in Fig. 5. The accelerating voltage is the vectorial sum of generator- and beam-induced voltage and remains nearly constant from $t =$

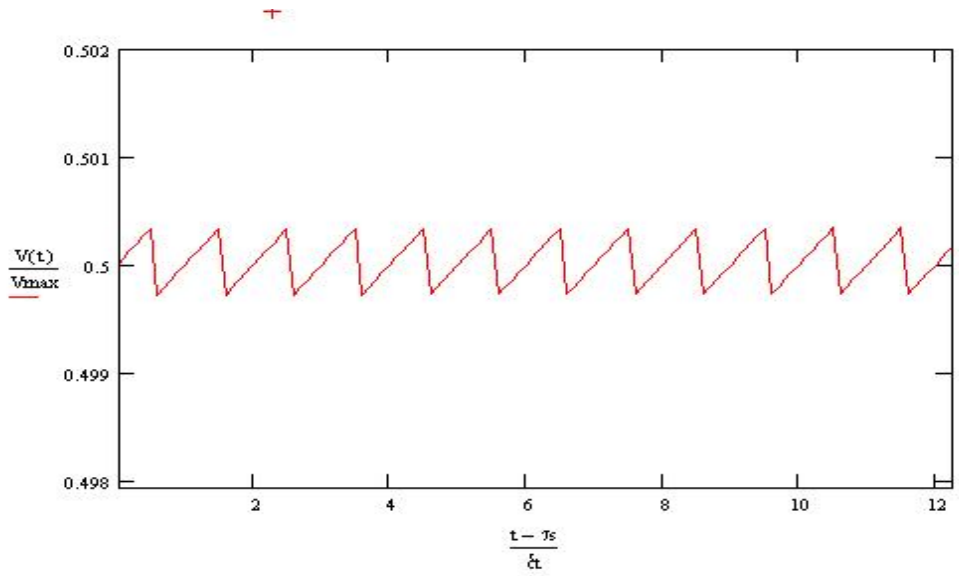

Figure 5: Bunch acts as delta function.

T_{inj} until $t = T_{end}$ at which time both generator power and beam are switched off. Then the cavity voltage decays according to

$$V_{acc}(t - T_{end}) = 0.5\, V_{max} \exp(-(t - T_{end})/\tau)\ . \tag{44}$$

A closer look at the plateau of the accelerating voltage reveals a sawtooth structure: each bunch causes an almost instantaneous drop of the cavity voltage which is then restored by the rising generator-induced voltage until the the next bunch arrives. The beam energy spread caused by the sawtooth structure is well below 0.1% for the example shown in Fig. 5. It can be further reduced by lowering the bunch charge and increasing the number of bunches in the train correspondingly.

Figure 5 illustrates how important it is to choose the proper cavity time constant for obtaining a constant accelerating voltage over the entire bunch train. Since $Q_{ext} \ll Q_0$ one gets in good approximation $\tau = 2Q_{ext}/\omega_0$ so the coupling strength of the input coupler (i.e. the winding ratio n of the equivalent transformer of Fig. 2) must be properly adjusted for the given accelerating field and beam current. In the TESLA couplers the central antenna is movable to permit such an adjustment.

2 Superconducting Radiofrequency cavities

Superconductivity was discovered in 1913 by Kammerlingh Omnes in Leiden. It was found that for mercury below a certain temperature (T = 4.2 K) no

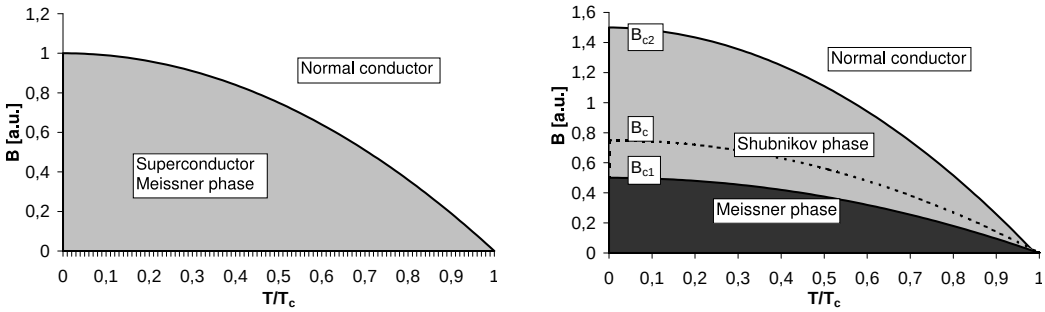

Figure 6: Phase diagrams for superconductors of type I (left) and type II (right).

ohmic resistance could be measured. By now a large number of elements and compounds (mainly alloys and ceramics) have been found showing this behaviour. For superconducting cavities niobium shows the most interesting properties. The general features of superconductivity as well as the special properties of niobium are described.

2.1 Characteristic length scales of superconductivity

2.1.1 Meissner-Ochsenfeld effect

Two different types of superconductors were discovered. They have certain common features, but differ also in some important ways. When the material is cooled below the critical temperature T_c the ohmic resistance vanishes below the measurement limit. In addition, any external magnetic field up to a critical field $B < B_{crit}$ is expelled. This magnetic field expulsion is called the Meissner-Ochsenfeld effect. This behaviour significantly differs from the properties of an ideal conductor where the field would be trapped inside the material. Even if the field is switched off, an ideal conductor would keep the magnetic field and become a permanent magnet as the currents induced by the field will continue to flow. From a thermodynamical point of view, one can define the thermodynamical critical field B_c:

$$G_n - G_s = \frac{1}{2\mu_0} V B_c^2 \tag{45}$$

Here one takes difference of the free enthalpy G in the normal- and the superconducting state respectively. Experimentally, B_c can be determined from the area below the magnetization curve of the material.

If the field exceeds a critical value B_c in a superconductors of type I the superconductivity breaks down and the normal conducting state is restored.

This critical field depends on the critical temperature:

$$B_c(T) = B_c(0)\left[1 - \left(\frac{T}{T_c}\right)^2\right] \tag{46}$$

For the second type of superconductor the magnetic field will start to penetrate the material above the lower critical field B_{c1}. Magnetic fluxons enter the material and their number increases with increasing field. If one raises the field further to a value of B_{c2} the material becomes normalconducting. The temperature dependence of the critical magnetic fields B_{c1} and B_{c2} is the same as for the B_c of a type I superconductor. This is shown in figure 6.

2.1.2 Coherence length in superconductors

For classical superconductors like lead or tin, a very successful microscopic theory was developed by Bardeen, Cooper and Schrieffer which is called BCS-theory [Bardeen et al. 1957]. They assumed that electrons begin to condense below T_c to pairs of electrons, the so called Cooper pairs. The two electrons in a pair have opposite momentum and spin. They experience an attractive force mediated via quantized lattice vibrations called phonons. This bound state of the two electrons is energetically favourable. As the overall spin of these two paired electrons is zero, many of these pairs can co-exist coherently, just like other bosons. The coherence length describes the distance over which the electrons are correlated. It is given by:

$$\xi_0 = \frac{\hbar v_F}{\Delta} \tag{47}$$

v_F denotes the velocity of the electrons near the Fermi energy and $2 \cdot \Delta$ is the energy necessary to break up a Cooper pair. Typical values for the coherence length in niobium are around 39 nm. If one interprets the coherence length as the size of a Cooper pair, one immediately sees that it spans over many lattice constants. Within the BCS theory the energy gap can be calculated:

$$\Delta = 1.76 k_B T_c \tag{48}$$

The exact value of factor (1.76) in the relation of the energy gap and the critical temperature is material dependent and for niobium one finds higher values of $\Delta = 1.9 k_B T_c$, which can be seen for example in figure 8. The number of Cooper pairs $n_{cooper} = n_s/2$ is temperature dependent and only at T = 0 K all conduction electrons are condensed into Cooper pairs. The superconducting electrons co-exist with their normalconducting counterparts. The number of normalconducting electrons is given by the Boltzmann factor:

$$n_e(T \to 0) \approx n_s(0) \exp\left(-\frac{\Delta(T)}{k_b T}\right) \tag{49}$$

2.1.3 London penetration depth

Even in a type I superconductor the magnetic field is not completely expelled, but penetrates into the material over a small distance, as otherwise the shielding current density would have to be infinitely large. The so-called London penetration depth is given by the characteristic length of the exponential decay of the magnetic field into the superconductor.

$$B(x) = B(0)e^{-\frac{x}{\lambda_L}} \tag{50}$$

Its value is

$$\lambda_L = \sqrt{\frac{m}{\mu_0 n_s c^2}} \tag{51}$$

where e is the charge of an electron, m its mass and n_s the number of superconducting charge carriers per unit volume. A typical value for the penetration depth in niobium is 32 nm. The theory did not allow for impurities in the material nor for a temperature dependence of the penetration depth. Gorter and Casimir introduced the two-fluid model where a coexistence of a normal- and superconducting fluid of charge carriers is postulated.

$$n_c = n_n + n_s \tag{52}$$

They suggested a temperature dependence of the superconducting charge carriers.

$$n_s(T) = n_s(0) \cdot \left(1 - \left(\frac{T}{T_c}\right)^4\right) \tag{53}$$

Combining equations 51 and 53, the penetration depth shows the following temperature dependence:

$$\lambda_L(T) = \lambda(0) \left(1 - \left(\frac{T}{T_c}\right)^4\right)^{-\frac{1}{2}} \tag{54}$$

The Ginzburg-Landau parameter is defined as:

$$\kappa = \frac{\lambda_L}{\xi_0} \tag{55}$$

κ allows to distinguish between the two types of superconductors:

$$\kappa < \frac{1}{\sqrt{2}} \qquad \text{Superconductor type-I} \tag{56}$$

$$\kappa > \frac{1}{\sqrt{2}} \qquad \text{Superconductor type-II} \tag{57}$$

Niobium has $\kappa \approx 1$ and is a weak type-II superconductor.

The role of impurities was studied by Pippard [Pippard 1953] was based on the evidence that the penetration depth depends on the mean free path of the electrons ℓ in the material. The dependence of ξ on the mean free path is given by:

$$\frac{1}{\xi} = \frac{1}{\xi_0} + \frac{1}{\ell} \tag{58}$$

He introduced an effective penetration depth:

$$\lambda_{eff} = \lambda_L \cdot \frac{\xi_0}{\xi} \tag{59}$$

Here again ξ_0 is the characteristic coherence length of the superconductor. This relation reflects that the superconducting penetration depth increases with a reduction of the mean free path [Waldram 1964]. For pure ("clean") superconductor ($\ell \to \infty$) one has $\xi = \xi_0$. In the limit of very impure ("dirty") superconductors where $\ell \ll \xi_0$, the relation becomes

$$\xi = \ell. \tag{60}$$

The mean free path in the niobium is strongly influenced by interstitial impurities like oxygen, nitrogen and carbon. This point will become relevant in chapter 2.4.5 where the quality factor of a cavity and its dependence on the accelerating field are discussed.

Experimental values	
Critical temperature T_c	9.2 K
Coherence length ξ_0	39 nm
London penetration depth λ_L	30 nm
GL parameter κ	0.8

Table 2: Superconducting properties of polycrystalline high-purity niobium [Bahte 1998, Padamsee et al. 1998].

2.2 Radiofrequency critical magnetic field

The above mentioned description of the critical magnetic field applies for the dc case. For microwaves in the GHz-regime the situation is more complicated, as the current changes its sign every 10^{-9} seconds. Calculations have shown that the Meissner state can persist beyond B_{c1}. If no nucleation centers are available the possibility of a metastable state exists and therefore a delayed entry of the magnetic field - the so-called superheated state - might occur. Possible nucleation centers for magnetic flux are surface defects like protrusions or normalconducting inclusions. Therefore the surface condition and roughness are very important to achieve the superheating.

The superheated field has been calculated on the basis of the Ginzburg-Landau equations [Matricon and Saint-James 1967]. The superheating field is given for different κ in [Piel 1989]:

$$\begin{aligned} B_{sh} &= 0.75 B_c \quad \text{for} \quad \kappa \gg 1 \\ B_{sh} &= 1.2 B_c \quad \text{for} \quad \kappa \approx 1 \\ B_{sh} &= \tfrac{1}{\sqrt{\kappa}} B_c \quad \text{for} \quad \kappa \ll 1 \end{aligned}$$

A superheating field has been observed in type-I when a defect-free surface was used [Doll and Graf 1967]. Measurements on type-I and type-II superconductors at various frequencies indicate that the superheating field indeed exists at temperatures close to the critical temperature. The results are shown in figure 7. This was confirmed in more recent measurements where on 1.3 GHz niobium cavities it was shown that the superheating state can be achieved if the temperature is close to T_c [Hays and Padamsee 1997]. At temperatures at 4.2 K or 2 K and correspondingly higher fields (compare equation 46) the superheated state has not yet been established probably because other effects limit the maximum field gradient. These are for example local defects, which limit the maximum achievable field due to thermal breakdown as is described in section 2.4.2. At 2 K the maximum field is in the order of B_{c1} or slightly higher.

Property	Experimental data [mT] at 4.2 K	Calculated field [mT] at 0 K	Calculated field [mT] at 2 K	E_{acc} [MV/m] at 2 K
B_{c1}	130	164	156	37
B_c	158	200	190	45
B_{sh}	190	240	230	54
B_{c2}	248	312	297	62

Table 3: Critical magnetic fields of high-purity niobium. The corresponding acceleration gradient for the TESLA cavities is also given [Bahte et al. 1997], [Bahte 1998].

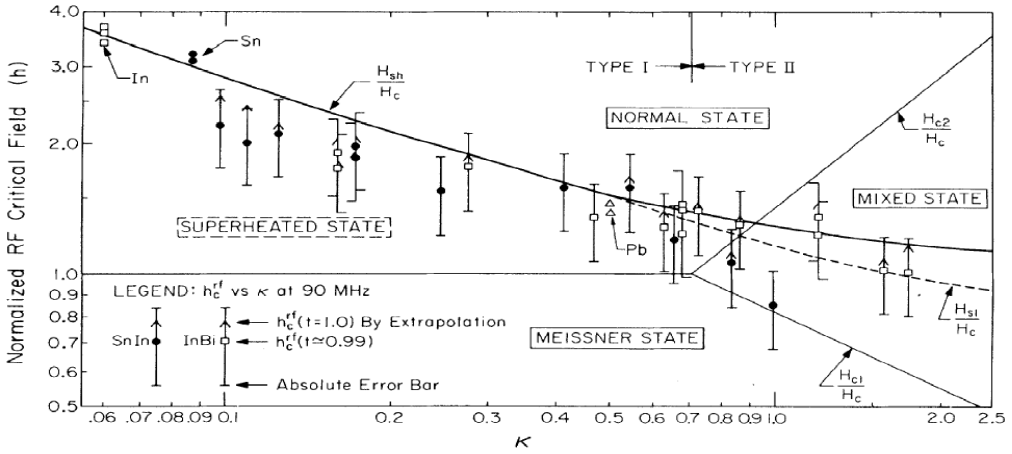

Figure 7: Measurements on the radiofrequency critical magnetic field in different superconducting alloys (SnIn, InBi) as a function of the Ginzburg-Landau parameter κ for temperatures near T_c [Yogi et al. 1977]. The curve $\frac{H_{sh}}{H_c}$ denotes the calculation by [Matricon and Saint-James 1967].

2.3 Microwave surface resistance

2.3.1 BCS resistance

Superconductors are free from energy dissipation in direct-current (dc) applications, but this is no longer true in alternating-current (ac) applications and particularly not in microwave fields. The reason is that the high-frequency magnetic field penetrates a thin surface layer and induces oscillations of the electrons which are not bound in Cooper pairs. The power dissipation caused by the motion of the unpaired electrons can be characterized by a surface resistance. In copper cavities the surface resistance is given by

$$R_{surf} = \frac{1}{\delta\sigma} \tag{61}$$

where δ is the skin depth and σ the conductivity of the metal.

The response of a superconductor to an ac field can be understood in the framework of the so-called two-fluid model[8]. An ac current in a superconductor is carried by Cooper-pairs (the superfluid component) as well as by

[8] A similar model is used to explain the unusual properties of liquid helium below 2.17 K in terms of a normal and a superfluid component.

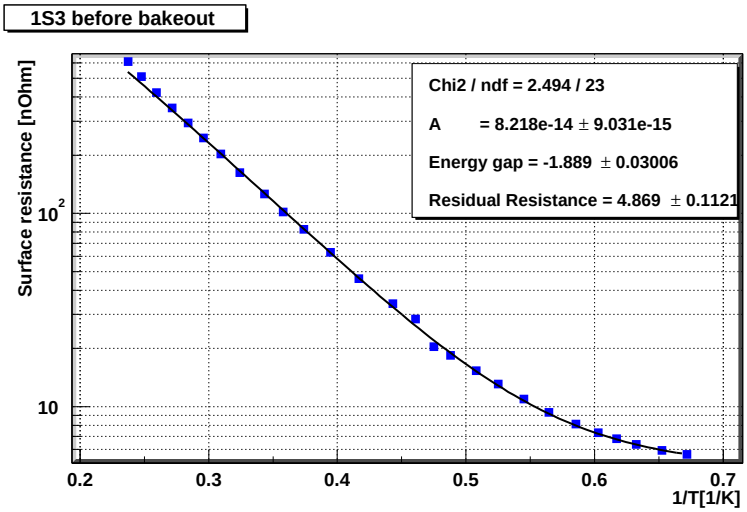

Figure 8: Measurement of the temperature dependence of the surface resistance of a single-cell niobium 1.3 GHz cavity. The fit to the curve results in an energy gap $\Delta = 1.889 \cdot k_b T_c$ and a residual resistance of 5 nΩ.

unpaired electrons (the normal component). Let us study the response to a periodic electric field. The normal current obeys Ohm's law

$$j_n = \sigma_n E_0 exp(-i\omega t) \tag{62}$$

while the Cooper pairs receive an acceleration

$$m_c \dot{v_c} = -2eE_0 exp(-i\omega t) \quad \Rightarrow \quad j_c = i\frac{n_c 4e^2}{m_c \omega} E_0 exp(-i\omega t)\ . \tag{63}$$

Here n_c is the density of Cooper pairs and $m_c = 2m_e$ their mass. If we write for for the total current density

$$j = j_n + j_c = \sigma E_0 exp(-i\omega t) \tag{64}$$

we get a complex conductivity:

$$\sigma = \sigma_n + i\sigma_c \quad \text{with} \quad \sigma_c = \frac{n_c 4e^2}{m_c \omega}\ . \tag{65}$$

The surface resistance is

$$R_{surf} = Re\left(\frac{1}{\sigma \lambda_L}\right) = \frac{1}{\lambda_L} \cdot \frac{\sigma_n}{\sigma_n^2 + \sigma_c^2}\ . \tag{66}$$

Now $\sigma_n \ll \sigma_c$ up to THz frequencies so one can disregard σ_n^2 in the denominator. The normal conductivity is proportional to the number n of unpaired electrons which, in analogy with an intrinsic semiconductor, depends exponentially on temperature:

$$n \propto \exp(-E_g/k_B T) = \exp(-\Delta \tag{67}$$

From this equation we

$$R_{BCS} \propto \frac{f^2}{T} \exp(-1.76\, T_c/T) \tag{68}$$

where f is the microwave frequency. In the two-fluid model of superconductors one can derive a refined expression for the surface resistance [Bonin 1996b, Weingarten 1995]

$$R_{\mathrm{BCS}} = \frac{C}{T} f^2 \sigma_n \Lambda^3 \exp(-1.76\, T_c/T)\ . \tag{69}$$

Here C is a constant, σ_n the normal-state conductivity of the material and Λ an effective penetration depth, given by $\Lambda = \lambda_L\sqrt{1+\xi_0/\ell}$; λ_L is the London penetration depth, ξ_0 the coherence length and ℓ the mean free path of the unpaired electrons. The fact that σ_n is proportional to the mean free path ℓ leads to the surprising conclusion that the surface resistance does not assume its minimum value when the superconductor is as pure as possible ($\ell \gg \xi_0$) but rather in the range $\ell \approx \xi_0$. For niobium the BCS surface resistance at 1.3 GHz amounts to about 800 nΩ at 4.2 K and drops to 15 nΩ at 2 K, see Fig. 8. The exponential temperature dependence is the reason why operation at 1.8–2 K is essential for achieving high accelerating gradients in combination with very high quality factors. Superfluid helium is an excellent coolant owing to its high heat conductivity.

The dependence of R_{BCS} on the mean free path can also be calculated: [Saito and Kneisel 1999]:

$$R_{BCS}(\ell) \propto \left(1+\frac{\xi_0}{\ell}\right)^{\frac{3}{2}} \cdot \ell \tag{70}$$

There exists a minimum of R_{BCS} on the mean free path ℓ. A more detailed calculation of the BCS theory shows that the two-fluid model gives a good approximation for $\ell < 500nm$ [Halbritter 1970] (see figure 9).

2.3.2 Residual resistance

The total surface resistance contains in addition a temperature independent part, which is called residual resistance R_{res}. The residual resistance is usually dominated by lattice imperfections, chemical impurities, adsorbed gases

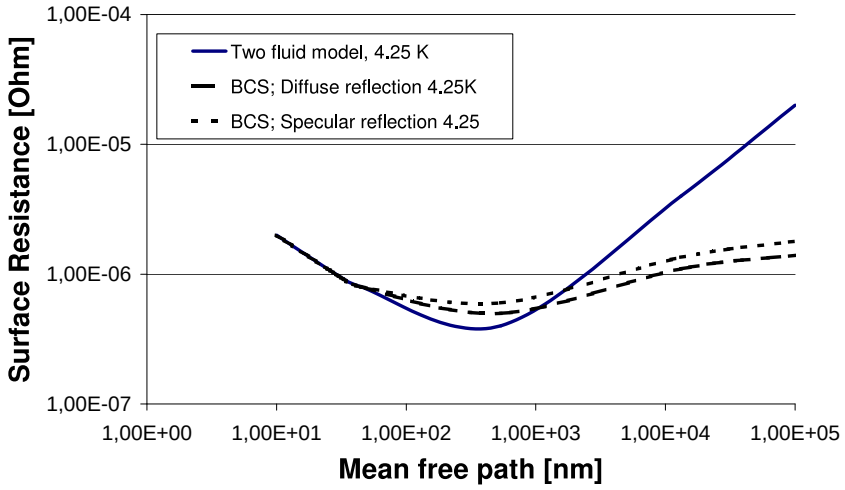

Figure 9: Calculated BCS surface resistance at 4.2K for 1.3 GHz plotted versus mean free path ℓ [Halbritter 1970]; this figure is taken from [Saito and Kneisel 1999].

and trapped magnetic field. Well prepared niobium surfaces show a residual resistance of a few nΩ (figure 8).

Absorbed gases can lead to a high residual resistance [Piosczyk 1974]. The dielectric properties of N_2 and O_2 are the reason for this behaviour. Minor contributions come from dielectric losses of the natural oxide Nb_2O_5. They have been estimated to be in the order of 1 nΩ [Palmer 1988] or below [Reschke 1995].

If a cavity is not shielded from the earth magnetic field its surface resistance is increased due to trapped magnetic fluxons. Those fluxons are trapped at impurities called pinning centers even though the superconductor tries to expel the magnetic field. The losses from fluxons can be calculated:

$$R_{fl} = \eta \frac{B_{ext}}{B_{c2}} R_{surf,nc} \tag{71}$$

B_{ext} is the external magnetic field and $R_{surf,nc}$ is resistivity of the material in the normalconducting state. $\eta \leq 1$ is a correction factor for the field expulsion. Measurements have shown that the trapping efficiency is very close to 1 even in high purity niobium [Bonin et al. 1992].

Any contamination of the surface with metallic parts (from screws, gaskets, etc.) or dielectric remnant from the surface treatment has to be avoided. It can enhance the residual RF losses to an intolerable level.

2.4 Limiting mechanisms in superconducting cavities

2.4.1 Diagnostic tools

Material science plays an important role to achieve the maximum gradient in high field accelerating cavities, both normal- ans superconducting. To achieve good reproducibility in the cavity performance it is mandatory to clearly identify loss mechanisms with advanced diagnostic techniques. Most of these tools are described in [Padamsee et al. 1998].

One very important diagnostic is the mapping of the outer cavity surface with temperature sensors (T-mapping). Systems consist either of rotating thermometer arms ([Pekeler et al. 1995]) or fixed sensors on the surface using a principle developed at Cornell University [Knobloch 1997]. The temperature maps allow to distinguish between localised hot spots due to foreign particle inclusions or multipacting, traces of field emitters or global heating effects. The resolution of the fixed T-mapping is a few mK. Usually the test setup also includes one (or more) X-ray sensors on top of the test cryostat. This is a good indicator for field emission. Sometimes this is supplemented with a sensitive electrometer which can detect electrons hitting the antenna used for monitoring the cavity field.

2.4.2 Thermal breakdown

Thermal breakdown can occur when a normalconducting defect starts to heat due to the induced ac currents. If the field is raised further the heat can lead to an increase of the temperature in the surrounding niobium material above its critical temperature T_c. As more material becomes normalconducting, more heat is generated and finally the cavity suffers a breakdown of superconductivity (see figure 10).

2.4.3 Heat flow in bulk niodium

Kapitza resistance When a defect-free niobium surface is heated with the radiofrequency power, the heat flows through an area A with heat current $\dot{Q}/A$. The temperature in the niobium decreases linearly if the temperature dependence of the thermal conductivity λ can be neglected as shown in figure 11. As superfluid helium has a very high thermal conductivity the temperature of the helium bath is nearly constant everywhere. Nevertheless, there exists a very small interface layer between the niobium and the helium of about 10-100 atomic layers (Kapitza layer) in which the temperature decreases exponentially from the temperature of the outer niobium surface to the bath temperature [Sciver 1986].

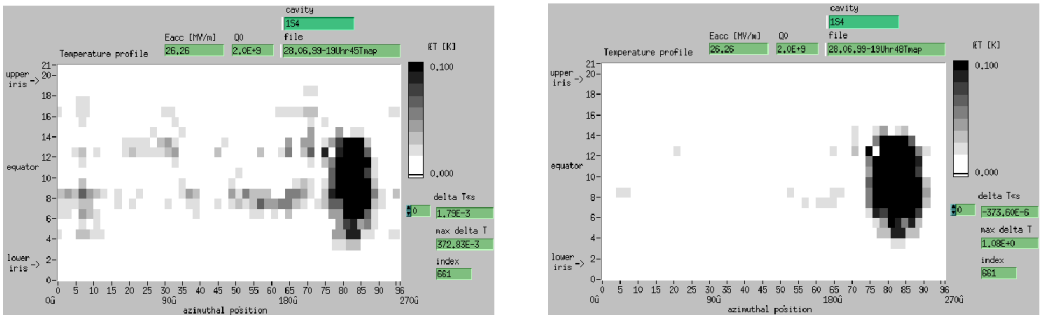

Figure 10: Quench location in an etched cavity. The left picture shows the breakdown with the incident power level adjusted to the minimum level needed for the breakdown. One can see both, the average heating in the high magnetic field region is in the order of 100 mK and the average heating in the thermal breakdown area (300 mK) . In the right picture more incident RF power was used so that the quench location heats up much more (1 K).

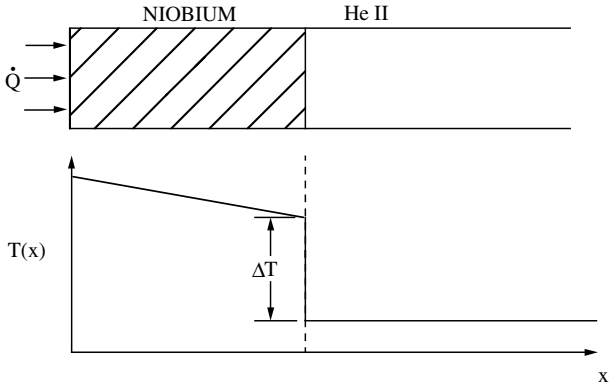

Figure 11: Distribution of the temperature in the niobium material and the superfluid helium. In the niobium the temperature decreases linearly, while in the helium bath the temperature is constant. In the interface layer the temperature drops quickly by an amount of ΔT to the temperature of the bath [Pekeler 1996].

The temperature ΔT in the interface is proportional to $\dot{Q}/A$:

$$\frac{\dot{Q}}{A} = h_{\mathrm{k}} \cdot \Delta T \; ; \tag{72}$$

The factor h_{k} is called the Kapitza conductivity. And depends strongly on the bath temperature. The relation is [Mittag 1973, Fouaidy et al. 1992]:

$$h_{\mathrm{k}} = c_{\mathrm{k}} \cdot {T_{\mathrm{B}}}^{n} \; . \tag{73}$$

Element	O	N	C	Ta	Zr
$\frac{\Delta\rho}{\Delta C}$ [10^{-11} Ωm/wt.ppm.]	2.64	3.49	3.33	0.12	0.6

Table 4: $\Delta\rho/\Delta C$ for different impurities in niobium [Hörmann 1986].

The values of c_k and n depend on the surface properties and the RRR of the niobium and are typically $0.5 < c_\mathrm{k} < 1.1$ and $2.5 < n < 3.8$.

Thermal conductivity The thermal conductivity plays an important role for the maximum breakdown field if the cavity has a normalconducting defect on the surface. This can also be a niobium particle with bad thermal contact to the surface or a niobium tip where the field enhancement leads to a breakdown of superconductivity. The microwave surface resistance increases strongly above $\mathrm{T}_c/2$ and reaches the value of normalconducting niobium at T_c. This is approximately 3 mΩ at 10 K.

One parameter to characterize the thermal conductivity of the niobium is the RRR, the residual (normalconducting) resistitivity ratio, which is defined as:

$$RRR = \frac{\rho_{nc}(300K)}{\rho_{nc}(4.2K)} \tag{74}$$

The specific electrical dc resistivity ρ consists according to Matthiessen's rule of a temperature dependent part $\rho(T)$ due to scattering with the lattice vibrations (phonons) and a residual resistance which is mainly due to impurity atoms [Schulze 1981]:

$$\rho_{nc}(T) = \rho_{res} + \rho_{phonon}(T) \tag{75}$$

For the temperature depending part one has $\rho(300K) = 1.46 \cdot 10^{-7}\Omega m$, $\rho(4.2K) = 8.7 \cdot 10^{-11}\Omega m$ [Fuss 1976]. The residual resistivity part is given by:

$$\rho_{res} = \sum_i \left(\frac{\Delta\rho}{\Delta C}\right)_i C_i \tag{76}$$

The coefficients for a few selected impurity elements are given in table 4.
To relate the RRR with mean free path, one could assume Drude's law:

$$\rho = \frac{m v_F}{n e^2 \ell} \tag{77}$$

As for cryogenic temperatures Drude's law is not applicable and the derivation of a analytical formula is difficult, one reverts to the empirical formula

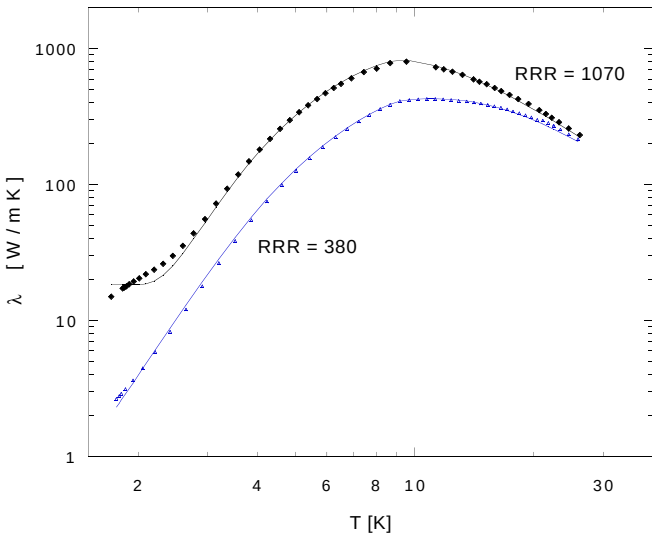

Figure 12: Measured heat conductivity in niobium as a function of temperature [Schilcher 1995]. Continuous curves: parametrization by B. Bonin, using the RRR and the average grain size as input parameters [Bonin 1996a]. These data do not show an enhancement at 2 K (the so-called "phonon peak") which was observed in some earlier experiments [Müller 1988a].

[Bonin 1996b]:

$$\ell \approx 2.65 \cdot RRR \qquad \text{where } \ell \text{ is given in nm} \tag{78}$$

There exists an empirical formula which holds for the thermal conductivity $\lambda_{thermal}$ [Padamsee et al. 1998]:

$$RRR \approx 4 \cdot \lambda_{thermal}(4.2K)[W/mK] \tag{79}$$

Some measurements on samples are shown in figure 12. Thermal model calculations (figure13) show that the thermal conductivity plays an important role to achieve very high RF magnetic fields. For the etched TESLA cavities, there is a considerable gain in performance with high RRR of 500 after post-purification since the defect size at 25 MV/m is then several ten μm. For fields of more than 150 mT (36 MV/m) the maximum defect size reduces down to about 10 μm.

Temperature rise on the outer cavity surface The temperature on the outside of the cavity, which can be measured using a thermometry system, depends on the thermal conductivity λ, the thickness of the niobium and the

Kapitza conductivity of the niobium-helium interface.

$$\frac{\dot{Q}}{A} = \frac{\lambda}{d}(T_\mathrm{i} - T_\mathrm{o}) = h_\mathrm{k}(T_\mathrm{o} - T_\mathrm{B}) \quad \Rightarrow \quad T_\mathrm{i} - T_\mathrm{B} = \frac{\dot{Q}}{A}\left(\frac{d}{\lambda} + \frac{1}{h_\mathrm{k}}\right) \tag{80}$$

T_i and T_o are the temperature of the inner and the outer surface, respectively. T_B is the helium bath temperature. With equation (73) and equation (80) one finds:

$$\Delta T_\mathrm{i} = \left(\frac{c_\mathrm{k} d}{\lambda} {T_\mathrm{B}}^n + 1\right) \Delta T_\mathrm{o} \; . \tag{81}$$

$\Delta T_\mathrm{i} = T_\mathrm{i} - T_\mathrm{B}$ and $\Delta T_\mathrm{o} = T_\mathrm{o} - T_\mathrm{B}$ denote the temperature differences on the inner and outer surface respectively. Measurements on samples have shown that the thermal conductivity of niobium with $RRR = 350$ in the temperature range of 1.5 K to 2 K is about $\lambda \approx 3$ W/(m·K) [Schilcher 1995]. For h_k one has at 1.8 K a value of 4000 W/(m^2 K) [Mittag 1973]. Together with a wall thickness of the niobium resonator of $d = 1.5$ mm the temperature increase on the inner surface ΔT_i is about three times the temperature increase on the outer surface ΔT_o.

$$\Delta T_\mathrm{i} \approx 3 \cdot \Delta T_\mathrm{o} \tag{82}$$

This is correct only for small temperature increases on the inner surface $\Delta T_\mathrm{i} = 1$ K, as the thermal conductivity depends strongly on the temperature. Thermal simulations are shown in figure 14 for a slightly different parameter set and show that the temperature increase is about 2 times higher on the inner surface than on the outer surface.

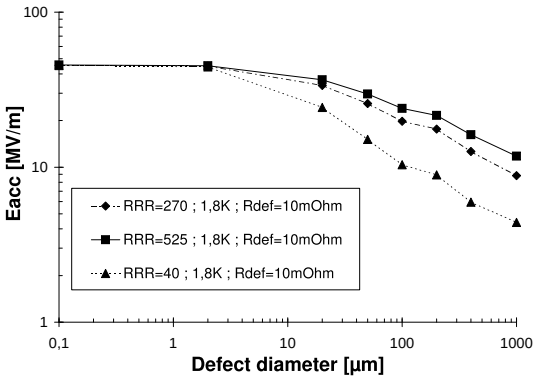

Figure 13: Simulation of the cavity performance in the presence of a normalconducting defect. Plotted is the maximum accelerating gradient below thermal breakdown as a function of defect diameter. These thermal simulations are done for 1.3 GHz and T_{bath} = 1.8 K assuming a critical magnetic field B_{crit} = 200 mT. The results indicate that at highest fields above 35 MV/m the defect size has to be extremely small [Reschke 1997].

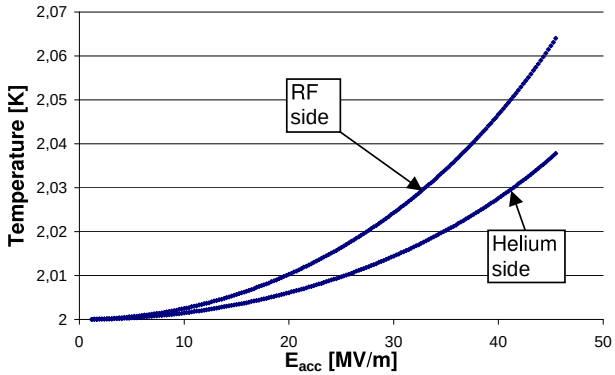

Figure 14: Temperatures on the RF side and the helium side of the niobium sheet. This simulation is done for B_{crit} = 240mT, a residual resistance of 6 nOhm, a niobium sheet thickness of 2.6 mm and a RRR=436 [Reschke 2001]. The $T_c(45MV/m)$ is 4.15 K.

2.4.4 Field emission

Field emission has been a serious limitation ever since accelerating cavities were built. Unfortunately, the superconducting cavities present no exception [Graber 1993], [Reece et al. 1995], [Reschke 1995], [Knobloch 1997], [Silari et al. 1999]. The high surface electric fields lead to electron emission from scratches or particles located on the surface via electron tunneling. Fowler and Nordheim developed a theory for the direct current case in which they found for the electron current emitted from a surface area A:

$$I_{FN} = A \cdot \frac{C}{\phi t^2(y)} E^2 \exp\left(-\frac{B\phi^{\frac{3}{2}} v(y)}{E}\right) \tag{83}$$

$B = 8\pi\sqrt{2m_e}/3he$ and $C = e^3/8\pi h$ are constants, ϕ is the workfunction of the metal. t(y) and v(y) are functions of $y = e^3E/4\pi\epsilon_0\phi^2$ which vary on slowly with electric field and can be set to 1 in first order approximation.

These electrons are subsequently accelerated inside the cavity and hit the walls. This process dissipates power and therefore can cause an exponential decrease of the quality factor with the accelerating field.

Although maximum care during assembly is taken at TTF it is by no means trivial to prevent field emission free nine-cell cavities. Several one-cell cavities have been assembled in the TTF infrastructure resulting in excellent performance without detectable field emission up to gradients of more than 40

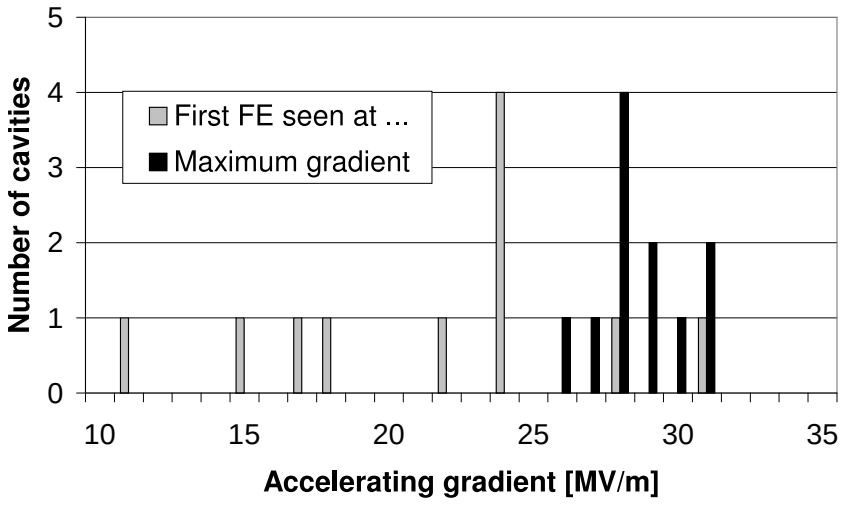

Figure 15: Accelerating gradient of the third production of TESLA nine-cell cavities shown in figure 28 when during the first power rise the first field emission signal is measured. Also shown is the maximum gradient of the test. A few cavities show no X-ray signal at all, whereas others show field emission at fields of 10 - 15 MV/m.

MV/m. The problem is more pronounced in multi-cell cavities. Their surface is larger, so that inevitably the chances to miss a field emitter during high pressure water rinsing are higher. In addition, electrons can be accelerated in a multi-cell through several cells, reach higher energies and therefore lead to a larger energy loss in the cavities [Stolzenburg 1996].

An interesting observation is that that the drop in quality factor is so similar in all the resonators shown in figure 28, although in figure 15 one clearly sees that field emission starts at significantly lower values of the accelerating field. We will see in the next part that the degradation is probably also due to another effect and that field emission contributes only partly to this behaviour.

2.4.5 Degradation of the quality factor without electron field emission

The curves shown in figure 28 are of similar shape, although the threshold for X-ray emission is quite different. Moreover in a few tests nine-cell cavities have shown virtually no x-rays at all (see figure 16). Hence field emission cannot be the only explanation for the quality factor degradation at high field. In 1-cell cavities at Saclay and other places a quality degradation at fields around 20 MV/m was observed without any sign of electron emission[9]. Apparently this "Q-drop without X-rays" shows up also in nine-cell cavities, as with the efforts of the TESLA collaboration the field emission thresholds have been pushed to a very high level.

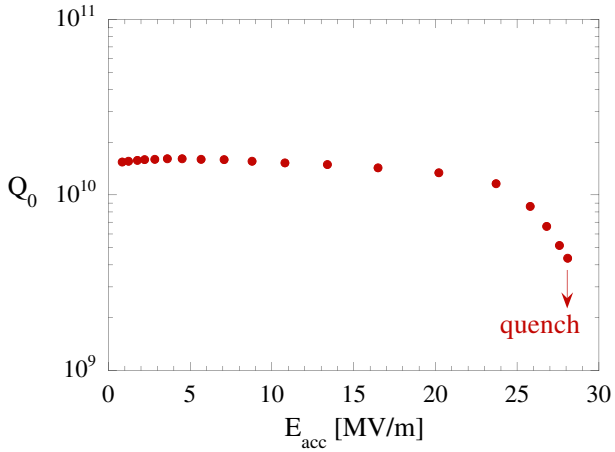

Figure 16: Excitation curve of a TESLA nine-cell cavity without field emission. The strong increase in surface resistance can be seen above 25 MV/m. Test was done at 2 K.

[9] See [Visentin et al. 1998], [Visentin et al. 1999], [Kneisel 1999], [Lilje et al. 1999].

This effect is under active study as the strong degradation can be cured by a small heating of the cavity at 100-120 degrees C. The diffusion of oxygen even at these temperatures is most likely changing the impuriy content enough inside the penetration depth to improve the gradient at high fields (see figure 17).

2.4.6 Multipacting

Another phenomenon related to free electrons inside the cavity vacuum that can cause a limitation for resonators is called "Multipacting" [10]. This stands for multiple impacting. If some electrons are impinging on the cavity wall, they can cause the emission of secondary electrons. Dependent on the secondary electron emission coefficient (SEEC) which typically shows an energy dependence (figure 19), the number of new electrons can be larger than 1. These particles are accelerated in the electromagnetic field and hit eventually the wall again. If this process takes place in resonance to the RF phase, an avalanche of electrons will occur and cause the cavity to breakdown. When the electrons travel forth and back between two points on the cavity surface, this is called two-point multipacting (see figure 18).

A typical place for two-point multipacting to occur is the equator region of elliptical cavities. Temperature maps have shown this in 352 MHz cavities [Weingarten et al. 1984]. Fortunately, niobium has an SEEC very close to 1 as can be seen in figure 19. The SEEC depends delicately on the adsorbed gas layers. Usually, multipacting barriers can be passed within a few minutes. This means that the electrons in the avalanche force gases

[10] See e.g. [Farnsworth 1934], [Hatch and Williams 1954], [Budliger and Laisne 1968].

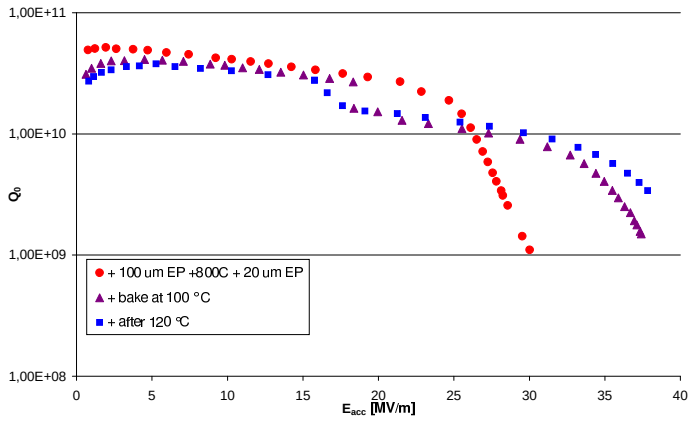

Figure 17: Improvement due to 'In-Situ'-Bakeout at 100 or 120 derees C. Test was done at 2 K.

to be desorbed. In this way the surface can be cleaned and the SEEC will drop below 1. This process is usually called "Conditioning" or "Processing". In a measurement at Cornell University it has been has reported that multipacting at frequencies of 1.5 GHz takes place at field levels of around 17 MV/m and confirmed the hot spots via temperature mapping [Knobloch 1997, Knobloch et al. 1997].

Although not a serious limitation for the chemically etched nine-cell cavities so far, it should be mentioned that multipacting is seen during nearly every test of a 1.3 GHz cavity at TTF. The field level is between 17 - 20 MV/m. Typically, conditioning takes a few minutes or less in a continuous wave (cw) test. Figure 20 shows T-maps taken at different stages during conditioning on electropolished one-cell cavities. The heating is seen to move along the equator during conditioning until the SEEC is reduced below 1 in the whole area affected by the multipacting.

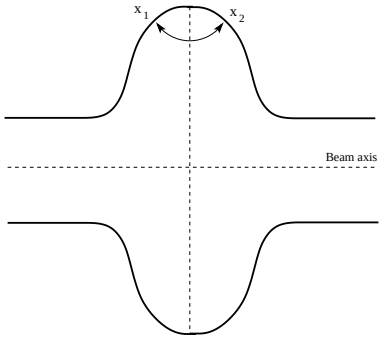

Figure 18: The two-point multipacting can occur in the equator region. Please note that the electron trajectories are exaggerated. The distance between the two impact points is typically in the order of a few millimeters to a centimeter [Knobloch 1997]. This is also visible in the temperature maps in figure 20.

3 Example for SRF cavity design and produciton: TTF cavities

3.1 Introduction

The main drawback of superconducting (sc) accelerating structures has traditionally been the low gradient of the cavities combined with the high cost of cryogenic equipment. At the time of the first TESLA workshop [Padamsee 1990] superconducting RF cavities in particle accelerators were usually operated in the 5 MV/m regime. Such low gradients would have

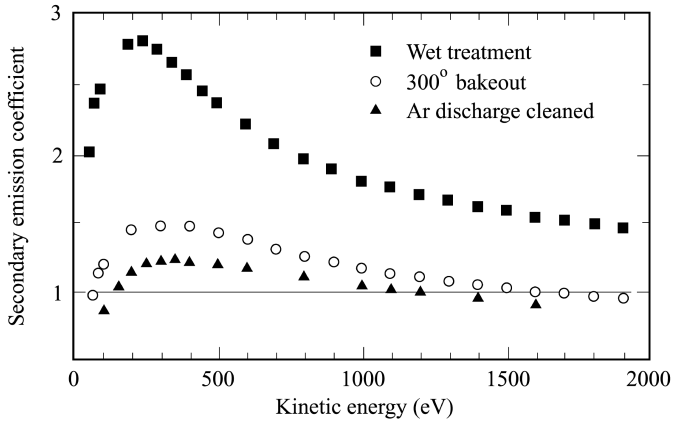

Figure 19: Secondary emission coefficient (SEEC) of niobium after different surface treatments [Piel 1989]. A bakeout at 300 °C leads to a strong reduction. This is due to the dissolution of the natural Nb_2O_5 layer which has a higher SEEC than niobium.

made a superconducting linear electron-positron collider of 500 GeV center-of-mass energy totally non-competitive with the normal-conducting colliders proposed in the USA and Japan. The ambitious design gradient of 25 MV/m was specified for TESLA. In the meantime this gradient has been safely established in multicell niobium cavities produced by industry, and in addition the cost per unit length of the linac has been considerably reduced by applying economical cavity production methods and by assembling many cavities in a long cryostat[11].

The TESLA cavities (see figure 21 and table 5) are similar in layout to the 5-cell 1.5 GHz cavities of the electron accelerator CEBAF which were developed at Cornell University and fabricated by an industrial company [Reece et al. 1995]. They exceeded the specified gradient of 5 MV/m considerably and hence offered the potential for further improvement. The CEBAF cavity manufacturing methods were adopted for TESLA with improved quality control of the superconducting material and of the fabrication methods, and important new steps were introduced in the cavity preparation collecting experiences from several different laboratories working on superconducting accelerating cavities (e.g. CEA Saclay, CERN, Cornell, KEK, Karlsruhe, Wuppertal and DESY):

[11] A recent review paper on the TESLA cavities can be found in [Aune et al. 2000]. A review paper on superconducting cavity science and technology can be found in [Padamsee 2001]. Also the developments on sputtered niobium films and other superconducting materials are reviewed.

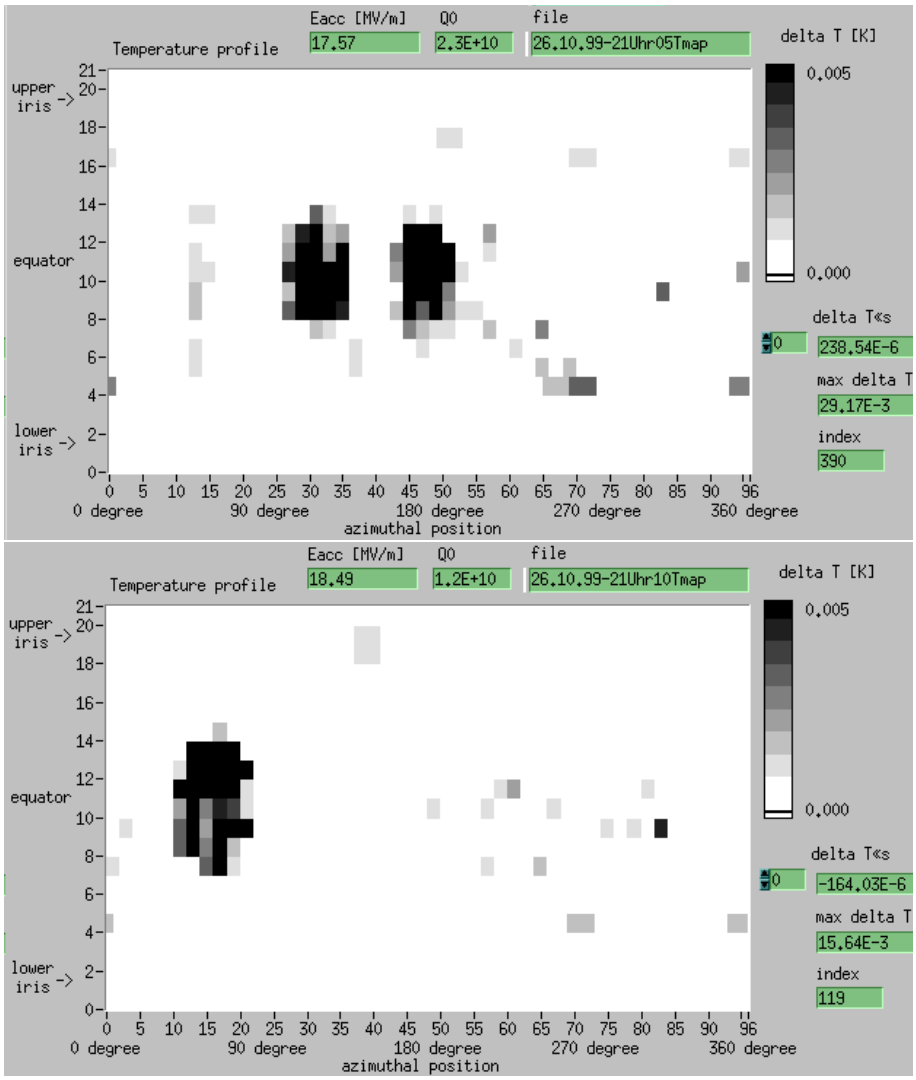

Figure 20: Temperature mappings on a 1.3 GHz one-cell cavity at different stages during conditioning of multipacting. After a few seconds of conditioning, the hot spot which can be seen at 17.5 MV/m is conditioned (top). A new area with heating appears at a slightly higher gradient of 18.5 MV/m (bottom). The full conditioning takes a few minutes. Note that the heating is typically much below 1 K, whereas in a thermal breakdown caused by material defects the temperature rises by several Kelvin.

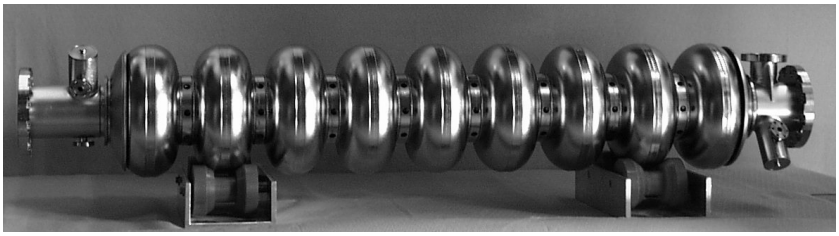

Figure 21: Picture of TESLA-type 9-cell cavity.

type of accelerating structure	standing wave
accelerating mode	TM_{010} , π mode
fundamental frequency	1300 MHz
design gradient E_{acc}	25 MV/m
quality factor Q_0	$> 5 \cdot 10^9$
active length L	1.038 m
number of cells	9
cell-to-cell coupling	1.87 %
iris diameter	70 mm
geometry factor	270 Ω
R/Q	1024 Ω
$E_{\text{peak}}/E_{\text{acc}}$	2.0
$B_{\text{peak}}/E_{\text{acc}}$	4.26 mT/(MV/m)
tuning range	± 300 kHz
$\Delta f/\Delta L$	315 kHz/mm
Lorentz force detuning at 25 MV/m	≈ 600 Hz
Q_{ext} of input coupler	$3 \cdot 10^6$
cavity bandwidth at $Q_{\text{ext}} = 3 \cdot 10^6$	430 Hz
RF pulse duration	1330 μs
repetition rate	5 Hz
fill time	530 μs
beam acceleration time	800 μs
RF power peak/average	208 kW/1.4 kW
number of HOM couplers	2

Table 5: TTF cavity design parameters [Brinkmann et al. 2001].

fundamental mode	TM_{010} , π mode
fundamental frequency	1300 MHz
active length L	11.46 cm
iris diameter	78 mm
geometry factor	270 Ω
R/Q	105 Ω
$E_{\mathrm{peak}}/E_{\mathrm{acc}}$	1.98
$B_{\mathrm{peak}}/E_{\mathrm{acc}}$	4.2 mT/(MV/m)

Table 6: One-cell cavity parameters.

- chemical removal of a thicker layer from the inner cavity surface
- a 1400°C annealing with titanium getter to improve the niobium heat conductivity and to homogenize the material
- rinsing with ultrapure water at high pressure (100 bar) to remove surface contaminants
- a closed chemistry system integrated in a clean-room facility
- destruction of field emitters by a technique called High Power Processing.
- better quality control of the niobium sheets with an eddy-current scanning method to detect foreign inclusions (e.g. tantalum grains)
- preparation of electron-beam welds with very tight specifications e.g. etching of the welding area, ultrapure water rinsing and clean room drying within less than 8 hours before welding to avoid contaminations in the weld

The application of these techniques, combined with an extremely careful handling of the cavities in a clean-room environment, has led to a significant increase in accelerating field.

The TESLA Test Facility (TTF) has been set up at DESY to provide the infra-structure for the chemical treatment, clean-room assembly and testing of industrially produced multicell cavities. An electron linac has been built as a test bed for the performance of the sc accelerating structures with an electron beam of high bunch charge. The linac is equipped with undulator magnets to generate FEL radiation in the VUV regime.

3.2 Design of the TESLA Cavities

3.2.1 Overview

The TTF cavity is a 9-cell standing wave structure of about 1 m length whose lowest TM mode resonates at 1300 MHz. A photograph is shown in Fig. 21. The cavity is made from solid niobium and is cooled by superfluid helium at 2 K. Each 9-cell cavity is equipped with its own titanium helium tank, a tuning system driven by a stepping motor, a coaxial rf power coupler capable of transmitting more than 200 kW, a pickup probe and two higher order mode couplers. To reduce the cost for cryogenic installations, eight cavities and a superconducting quadrupole are mounted in a common vacuum vessel and constitute the so-called cryomodule of the TTF linac, shown in Fig. 23. Within the module the cavity beam pipes are joined by stainless steel bellows and flanges with metallic gaskets. The cavities are attached to a rigid 300 mm diameter helium supply tube which provides positional accuracy of the cavity axes of better than 0.5 mm. Invar rods ensure that the distance between adjacent cavities remains constant during cooldown. Radiation shields at 5 K and 60 K together with 30 layers of superinsulation limit the static heat load on the 2 K level to less than 3 W for the 12 m long module.

3.2.2 Layout of the TESLA cavities

Choice of frequency The losses in a microwave cavity are proportional to the product of conductor area and surface resistance. For a given length of a multicell resonator, the area scales with $1/f$ while the surface resistance of a superconducting cavity scales with f^2 for $R_{\mathrm{BCS}} \gg R_{\mathrm{res}}$ and is independent of f for $R_{\mathrm{BCS}} \ll R_{\mathrm{res}}$. At an operating temperature $T = 2$ K the BCS term dominates above 3 GHz and hence the losses grow linearly with frequency whereas for frequencies below 300 MHz the residual resistance dominates and the losses grow with $1/f$. To minimize the dissipation in the cavity wall one should therefore select f in the range 300 MHz to 3 GHz.

Cavities in the 350 to 500 MHz regime are in use in electron-positron storage rings. Their large size is advantageous to suppress wake field effects and higher order mode losses. However, for a linac of several 10 km length the niobium and cryostat costs for these bulky cavities would be prohibitive, hence a higher frequency has to be chosen. Considering material costs $f =$ 3 GHz might appear the optimum but there are compelling arguments for choosing about half this frequency.

- The wake fields losses scale with the second to third power of the fre-

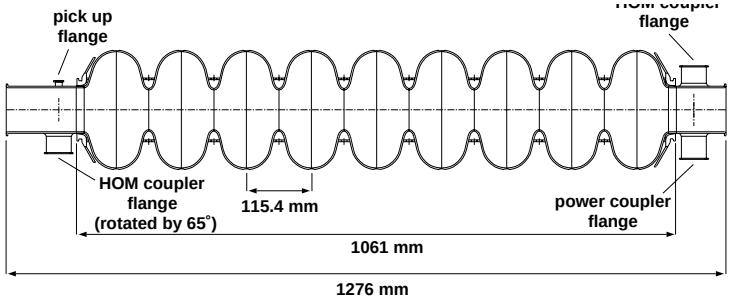

Figure 22: Side view of the 9-cell TTF cavity with the ports for the main power coupler and two higher-order mode (HOM) couplers.

quency ($W_\parallel \propto f^2$, $W_\perp \propto f^3$). Beam emittance growth and beam-induced cryogenic losses are therefore much higher at 3 GHz.

- The f^2 dependence of the BCS resistance sets an upper limit[12] of about 30 MV/m at 3 GHz, hence choosing this frequency would definitely preclude a possible upgrade of TESLA to 35–40 MV/m.

The choice for 1.3 GHz was motivated by the availability of high power klystrons.

Cavity geometry A multicell resonator is advantageous for maximizing the active acceleration length in a linac of a given size. With increasing number of cells per cavity, however, difficulties arise from trapped modes, uneven field distribution in the cells and too high power requirements on the input coupler. Extrapolating from the experience with 4-cell and 5-cell cavities a 9-cell structure appeared manageable. A side view of the TTF cavity with the beam tube sections and the coupler ports is given in Fig. 22.

The design of the cell shape was guided by the following considerations:

- a spherical contour near the equator with low sensitivity for multipacting,
- minimization of electric and magnetic fields at the cavity wall to reduce the danger of field emission and thermal breakdown,
- a large iris radius to reduce wake field effects.

[12] See Fig. 11.22 in [Padamsee et al. 1998].

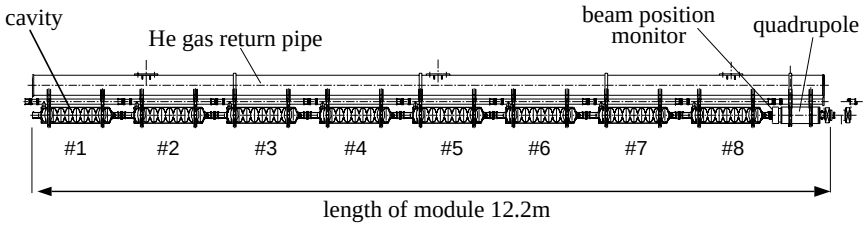

Figure 23: Cryogenic module of the TESLA Test Facility linac comprising eight 9-cell cavities and a superconducting quadrupole.

The shape of the cell was optimized using the code URMEL [Laustroër et al. 1987]. The resonator is operated in the π mode with 180° phase difference between adjacent cells. The longitudinal dimensions are determined by the condition that the electric field has to be inverted in the time a relativistic particle needs to travel from one cell to the next. The separation between two irises is therefore $c/(2f)$. The iris radius R_{iris} influences the cell-to-cell coupling[13] k_{cell}, the excitation of higher order modes and other important cavity parameters, such as the ratio of the peak electric (magnetic) field at the cavity wall to the accelerating field and the ratio (R/Q) of shunt impedance to quality factor. For the TESLA Test Facility cavities $R_{\mathrm{iris}} = 35$ mm was chosen, leading to $k_{\mathrm{cell}} = 1.87\,\%$ and $E_{\mathrm{peak}}/E_{\mathrm{acc}} = 2$. The most important parameters are listed in Table 5.

The contour of a half-cell is shown in Fig. 24. It is composed of a circular arc around the equator region and an elliptical section near the iris. The dimensions are listed in Table 7. The half-cells at the end of the 9-cell resonator need a slightly different shape to ensure equal field amplitudes in all 9 cells. In addition there is a slight asymmetry between left and right end cell which prevents trapping of higher-order modes (see Sect. 4.3).

Lorentz-force detuning and cavity stiffening The electromagnetic field exerts a Lorentz force on the currents induced in a thin surface layer. The resulting pressure acting on the cavity wall

$$p = \frac{1}{4}(\mu_0 H^2 - \varepsilon_0 E^2) \tag{84}$$

[13]The coupling coefficient is related to the frequencies of the coupled modes in the 9-cell resonator by the formula $f_n = f_0/\sqrt{1 + 2\,k_{\mathrm{cell}}\cos(n\pi/9)}$ where f_0 is the resonant frequency of a single cell and $1 \le n \le 9$.

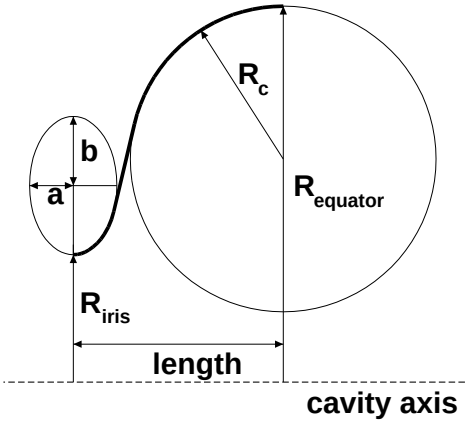

Figure 24: Contour of a half cell.

cavity shape parameter	midcup	endcup 1	endcup 2
equator radius $R_{\text{equat.}}$	103.3	103.3	103.3
iris radius R_{iris}	35	39	39
radius R_{arc} of circular arc	42.0	40.3	42
horizontal half axis a	12	10	9
vertical half axis b	19	13.5	12.8
length l	57.7	56.0	57.0

Table 7: Half-cell shape parameters (all dimensions in mm).

leads to a deformation of the cells in the μm range and a change ΔV of their volume. The consequence is a frequency shift according to Slater's rule

$$\frac{\Delta f}{f_0} = \frac{1}{4W} \int_{\Delta V} (\varepsilon_0 E^2 - \mu_0 H^2) dV \ . \tag{85}$$

Here

$$W = \frac{1}{4} \int_V (\varepsilon_0 E^2 + \mu_0 H^2) dV \tag{86}$$

is the stored energy and f_0 the resonant frequency of the unperturbed cavity. The computed frequency shift at 25 MV/m amounts to 900 Hz for an unstiffened cavity of 2.5 mm wall thickness. The bandwidth of the cavity equipped with the main power coupler ($Q_{\text{ext}} = 3 \cdot 10^6$) is about 430 Hz, hence a reinforcement of the cavity is needed. Niobium stiffening rings are welded in between adjacent cells. They reduce the frequency shift to about 500 Hz for a 1.3 ms long rf pulse[14], see Fig. 37.

The deformation of the stiffened cell is negligible near the iris where the electric field is large, but remains nearly the same as in the unstiffened cell near the equator where the magnetic field dominates. The deformation in this region can only be reduced by increasing the wall thickness.

Magnetic Shielding The ambient magnetic field must be shielded to a level of about a μT to reduce the magnetic surface resistance to a few nΩ. This is accomplished with a two-stage passive shielding, provided by the conventional steel vacuum vessel of the cryomodule and a high-permeability cylinder around each cavity. To remove the remanence from the steel vessel the usual demagnetization technique is applied. The resulting attenuation of the ambient field is found to be better than expected from a cylinder without any remanence. The explanation is that the procedure does not really demagnetize the steel but rather *remagnetizes* it in such a way that the axial component of the ambient field is counteracted. This interpretation (see also ref. [Albach and Voss 1957]) becomes obvious if the cylinder is turned by 180°: in that case the axial field measured inside the steel cylinder is almost twice as large as the ambient longitudinal field component, see Fig. 25a.

The shielding cylinders of the cavities are made from Cryoperm[15] which retains a high permeability of more than 10000 when cooled to liquid helium temperature. Figure 25b shows the measured horizontal, vertical and axial components inside a cryoperm shield at room temperature, which was exposed to the Earth's field. The combined action of remagnetized vacuum

[14] Part of this shift is due to an elastic deformation of the tuning mechanism.

[15] Cryoperm is made by Vacuumschmelze Hanau, Germany.

vessel and cryoperm shield is more than adequate to reduce the ambient field to the level of some μT. An exception are the end cells of the first and the last cavity near the end of the cryomodule where the vessel is not effective in attenuating longitudinal fields. Here an active field compensation by means of Helmholtz coils could reduce the fringe field at the last cavity to a harmless level.

3.2.3 Cavity fabrication

Choice of superconductor The existing large scale applications of superconductors in accelerators are twofold, in magnets and in accelerating cavities. While there are some common requirements like the demand for as high a critical temperature as possible[16] there are also characteristic differences. In magnets operated with a dc or a low-frequency ac current the so-called "hard" superconductors are needed featuring high upper critical magnetic fields (15–20 T) and strong flux pinning in order to obtain high critical current density; such properties can only be achieved using alloys like niobium-titanium or niobium-tin. In microwave applications the limitation of the superconductor is not given by the upper critical field but rather by the so-called "superheating field" which is well below 1 T for all known superconductors. Moreover, strong flux pinning appears undesirable in microwave cavities as it is coupled with hysteretic losses. Hence a "soft" superconductor must be used and pure niobium is still the best candidate although its critical temperature is only 9.2 K and the superheating field about 240 mT. Niobium-tin (Nb_3Sn) looks more favorable at first sight since it has a higher critical temperature of 18 K and a superheating field of 400 mT; however, the gradients achieved in Nb_3Sn coated single-cell copper cavities were below 15 MV/m, probably due to grain boundary effects in the Nb_3Sn layer [Müller 1988a]. For these reasons the TESLA collaboration decided to use niobium as the superconducting material, as in all other large scale installations of sc cavities. Here two alternatives exist: the cavities are fabricated from solid niobium sheets or a thin niobium layer is sputtered onto the inner surface of a copper cavity. Both approaches have been successfully applied, the former at Cornell (CESR), KEK (TRISTAN), DESY (PETRA, HERA), Darmstadt (SDALINAC), Jefferson Lab (CEBAF) and other laboratories, the latter in particular at CERN in the electron-positron storage ring LEP. From the test results on existing cavities the solid-niobium

[16] The High-T_c ceramic superconductors have not yet found widespread application in magnets mainly due to technical difficulties in cable production and coil winding. Cavities with High-T_c sputter coatings on copper have shown much inferior performance in comparison to niobium cavities.

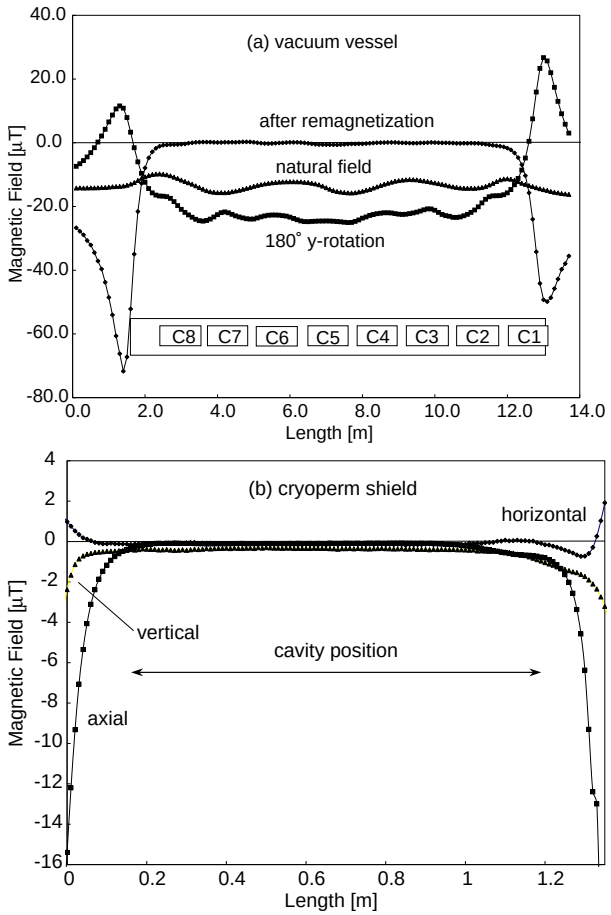

Figure 25: Shielding of the Earth's magnetic field. (a) Shielding of axial component by the steel vacuum vessel of the cryomodule. Shown is also the arrangement of the cavity string in the vessel. (b) Shielding of the axial, horizontal and vertical field components by the cryoperm cylinder surrounding the cavity (measured without vacuum vessel).

Impurity content in ppm (wt)				Mechanical Properties	
Ta	≤ 500	H	≤ 2	Residual resistivity ratio RRR	≥ 300
W	≤ 70	N	≤ 10	grain size	≈ 50 μm
Ti	≤ 50	O	≤ 10	yield strength	> 50 MPa
Fe	≤ 30	C	≤ 10	tensile strength	> 100 MPa
Mo	≤ 50			elongation at break	30 %
Ni	≤ 30			Vickers hardness HV 10	≤ 50

Table 8: Technical specification for niobium used in TTF cavities.

approach promised higher accelerating gradients, hence it was adopted as the baseline for the TTF cavity R&D program.

Niobium properties Niobium of high purity is needed. Tantalum with a typical concentration of 500 ppm is the most important metallic impurity. Among the interstitially dissolved impurities oxygen is dominant due to the high affinity of Nb for O_2 above 200°C. Interstitial atoms act as scattering centers for the unpaired electrons and reduce the RRR and the thermal conductivity, see section 2.4.2. The niobium ingot is highly purified by several remelting steps in a high vacuum electron beam furnace. This procedure reduces the interstitial oxygen, nitrogen and carbon contamination to a few ppm. The niobium specification for the TTF cavities is listed in Table 8.

After forging and sheet rolling, the 2.8 mm thick Nb sheets are degreased, a 5 μm surface layer is removed by etching and then the sheets are annealed for 1–2 hours at 700–800°C in a vacuum oven at a pressure of 10^{-5} – 10^{-6} mbar to achieve full recrystallization and a uniform grain size of about 50 μm.

Deep drawing and electron-beam welding The 9-cell resonators are made from 2.8 mm thick sheet niobium. Half-cells are produced by deep-drawing. The dies are usually made from a high yield strength aluminium alloy. To achieve the small curvature required at the iris an additional step of forming, e.g. coining, may be needed. The half-cells are machined at the iris and the equator. At the iris the half cell is cut to the specified length (allowing for weld shrinkage) while at the equator an extra length of 1 mm is left to retain the possibility of a precise length trimming of the dumb-bell after frequency measurement (see below). The accuracy of the shape is controlled by sandwiching the half-cell between two metal plates and measuring the resonance frequency. The half-cells are thoroughly cleaned by

ultrasonic degreasing, 20 μm chemical etching and ultra-pure water rinsing. Two half-cells are then joined at the iris with an electron-beam (EB) weld to form a "dumb-bell". The EB welding is usually done from the inside to ensure a smooth weld seam at the location of the highest electric field in the resonator. Since niobium is a strong getter material for oxygen it is important to carry out the EB welds in a sufficiently good vacuum. Tests have shown that $RRR = 300$ niobium is not degraded by welding at a pressure of less than $5 \cdot 10^{-5}$mbar.

The next step is the welding of the stiffening ring. Here the weld shrinkage may lead to a slight distortion of the cell shape which needs to be corrected. Afterwards, frequency measurements are made on the dumb-bells to determine the correct amount of trimming at the equators. After proper cleaning by a 30 μm etching the dumb-bells are visually inspected. Defects and foreign material imprints from previous fabrication steps are removed by grinding. After the inspection and proper cleaning (a few μm etching followed by ultra-clean water rinsing and clean room drying), eight dumb-bells and two beam-pipe sections with attached end half-cells are stacked in a precise fixture to carry out the equator welds which are done from the outside. The weld parameters are chosen to achieve full penetration. A reliable method for obtaining a smooth weld seam of a few mm width at the inner surface is to raster a slightly defocused beam in an elliptic pattern and to apply 50 % of beam power during the first weld pass and 100 % of beam power in the second pass.

3.2.4 Cavity treatment

Experience has shown that a damage layer in the order of 100 μm has to be removed from the inner cavity surface to obtain good RF performance in the superconducting state [17]. The standard method applied at DESY and many other laboratories is called Buffered Chemical Polishing (BCP), using an acid mixture of HF (48 %), HNO_3 (65 %) and H_3PO_4 (85 %) in the ratio 1:1:2 (at CEBAF the ratio was 1:1:1). The preparation steps adopted at DESY for the industrially produced TTF cavities are as follows. A layer of 80 μm is removed by BCP from the inner surface, 30 μm from the outer surface[18]. The cavities are rinsed with ultra-clean water and dried in a class 100 clean

[17] The preparation of the superconducting cavities is very different from its normalconducting counterparts like NLC or CLIC, where such a long etching would destroy the very accurate mechanically manufactured surface.

[18] These numbers are usually determined by weighing the cavity before and after etching and represent therefore the average over the whole surface. Frequency measurements indicate that more material is etched away at the iris than at the equator.

room. The next step is a two-hour annealing at 800°C in an Ultra High Vacuum (UHV) oven which serves to remove dissolved hydrogen from the niobium and relieves mechanical stress in the material. In the initial phase of the TTF program many cavities were tested after this step, applying a 20 μm BCP and ultra-clean water rinsing before mounting in the cryostat and cooldown.

Presently, the cavities are rinsed with clean water after the 800°C treatment and then immediately transferred to another UHV oven in which they are heated to 1350–1400°C. To capture the oxygen coming out of the niobium and to prevent oxidation by the residual gas in the oven (pressure $< 10^{-7}$mbar) a thin titanium layer is evaporated on the inner and outer cavity surface, Ti being a stronger getter than Nb. The high-temperature treatment with Ti getter is often called post-purification. The RRR increases by about a factor of 2 to values around 500. The titanium layer is removed afterwards by a 80 μm BCP of the inner surface. A BCP of about 30 μm is applied at the outer surface since the thermal interface resistance ("Kapitza resistance ") of titanium-coated niobium immersed in superfluid helium is about a factor of 2 larger than that of pure niobium [Boucheffa et al. 1995]. After final heat treatment and BCP the cavities are mechanically tuned to adjust the resonance frequency to the design value and to obtain equal field amplitudes in all 9 cells. This is followed by a slight BCP, three steps of high-pressure water rinsing (100 bar) and drying in a class 10 clean room. As a last step, the RF test is performed in a superfluid helium bath cryostat.

A severe drawback of the post-purification is the considerable grain growth accompanied with a softening of the niobium. Postpurified-treated cavities are quite vulnerable to plastic deformation and have to be handled with great care.

3.3 Results on Cavity Performance and Quality Control Measures

3.3.1 Results on cavity performance at TTF

Figure 26 shows the excitation curve of the best 9-cell resonator measured so far; plotted is the quality factor Q_0 as a function of the accelerating electric field E_{acc}. An almost constant and high value of $2 \cdot 10^{10}$ is observed up to 25 MV/m.

The importance of various cavity treatment steps for arriving at such a good performance are illustrated in the next figure. A strong degradation is usually observed if a foreign particle is sticking on the cavity surface, leading either to field emission of electrons or to local overheating in the RF field.

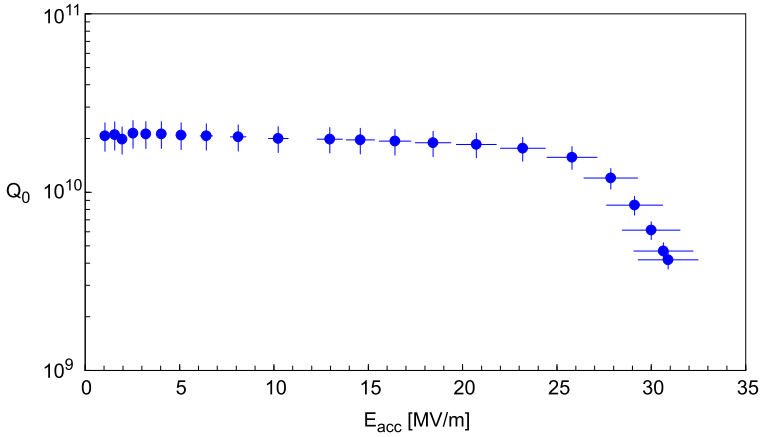

Figure 26: Excitation curve of the best chemically etched TESLA 9-cell cavity measured up to date. The cavity was cooled by superfluid helium of 2 K [Brinkmann et al. 2001].

At Cornell University an *in situ* method for destroying field emitters was invented [Graber et al. 1994], called high power processing (HPP), which in many cases can improve the high-field capability, see Fig. 27a. Removal of field-emitting particles by high-pressure water rinsing, a technique developed at CERN [Bernard et al. 1992], may eventually improve the excitation curve (Fig. 27b). The beneficial effect of a 1400°C heat treatment, first tried out at Cornell [Padamsee et al. 1990], Wuppertal [Müller 1988b] and later in Saclay [Safa et al. 1995], is seen in Fig. 27c. Finally, an incomplete removal of the titanium surface layer in the BCP following the 1400°C heat treatment may strongly limit the attainable gradient. Here additional BCP is of advantage (Fig. 27d).

From the last TTF cavity production series, which is produced by one company, 9 cavities have been tested up to date (see Fig. 28). They exceed the TESLA-500 specification: the average gradient at $Q_0 \geq 1 \cdot 10^{10}$ is 26.1± 2.3 MV/m and the average quality factor at the design gradient of 23.5 MV/m is $Q_0 = (1.39 \pm 0.35) \cdot 10^{10}$.

The reproducibility of the cavity performance is excellent. The curves of all cavities show very similar features. The maximum achievable gradient is clearly above 25 MV/m. The quality factor Q_0 is nearly constant up to an accelerating gradient of between 20 and 25 MV/m. In this region the real part of the surface resistance increases strongly. The final limit of most of these cavities is a thermal breakdown (quench). In some cavities it was not possible to get to this quench limit due to the available RF power in the

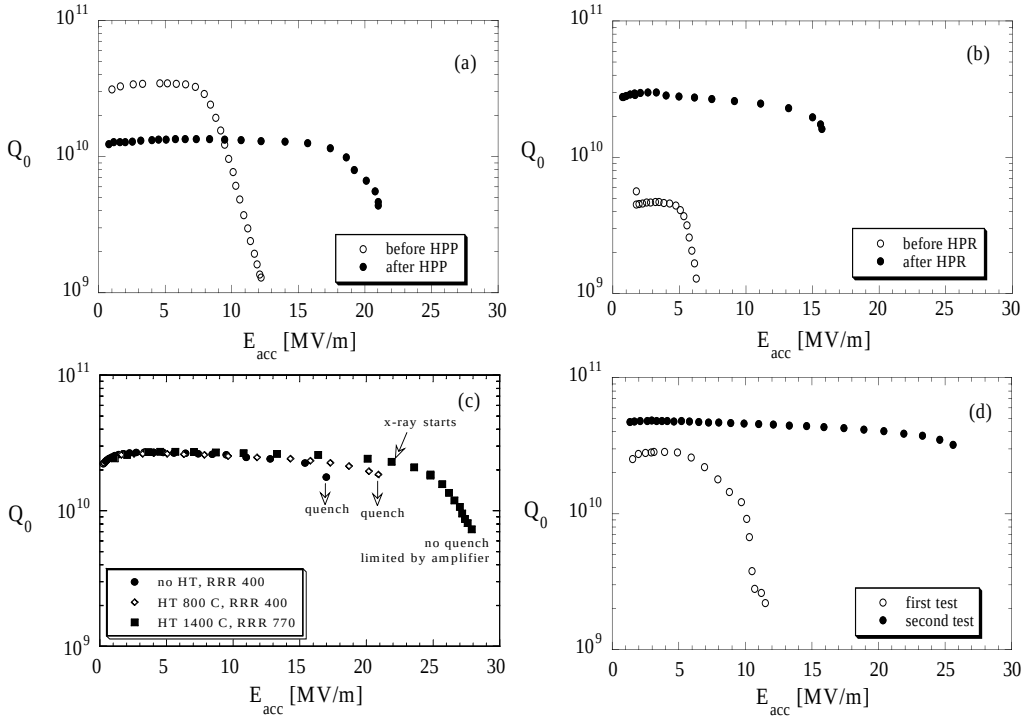

Figure 27: Improvement in cavity performance due to various treatments: (a) high power processing, (b) high pressure water rinsing, (c) successive application of 800°C and 1400°C heat treatment, (d) removal of surface defects or titanium in grain boundaries by additional BCP. All tests were done at 1.8 K [Aune et al. 2000].

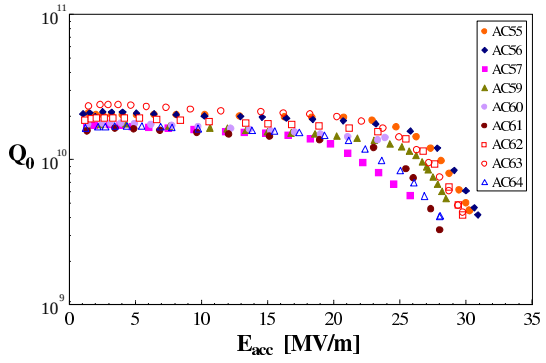

Figure 28: Excitation curves of cavities of the last TTF production. Tests were done at 2 K [Brinkmann et al. 2001].

continuous wave (cw) tests[19]. In Fig. 29 the performance of the cavities in the three production series is shown. The average gradient exhibits a clear trend towards higher values, and the width of the distribution is shrinking. It is obvious that the most recent cavities exceed the 23.5 MV/m operating gradient of TESLA-500 by a comfortable safety margin. Is is supported by the results in the high power tests, where a some cavities have been operated at more than 30 MV/m (Figure 30).

These values show that a clear improvement has been achieved with the above mentioned procedures. Still, most of the cavities are limited to gradients well below 35 MV/m corresponding to a maximum surface magnetic field of around 150 mT. Since the critical field of niobium at temperatures close to T_c is identical to B_{sh} [Hays and Padamsee 1997], it is a widespread believe that accelerating gradients of more than 50 MV/m ($B_{sh}(2K) > 200$ mT) in a perfect cavity could be achieved. The TESLA collaboration now aims to achieve gradients of 35 MV/m for the upgrade of the center-of-mass energy of the linac to 800 GeV. Therefore it is necessary to look closely at the limiting mechanisms of the cavities where known material[20] or fabrication defects can be excluded due to the tight specifications available.

3.4 Cavities of Higher Gradients

Both the TESLA collider and the X-ray FEL would profit from the development of cavities which can reach higher accelerating fields (i.e. higher particle energies) and higher quality factors (i.e. reduced operating costs of the accelerators). The TESLA design energy of 250 GeV per beam requires a gradient of 25 MV/m in the present nine-cell cavities. The results shown in Sect. 3.3.1 demonstrate that TESLA could indeed be realized with a moderate improvement in the present cavity fabrication and preparation methods. However, for particle physics an energy upgrade of the collider would be of highest interest, and hence there is a strong motivation to push the field capability of the cavities closer to the physical limit of about 50 MV/m which is determined by the superheating field of niobium. Three main reasons are known why the theoretical limit has not yet been attained in multicell resonators: (1) foreign material contamination in the niobium, (2) insufficient quality and cleanliness of the inner rf surface, (3) insufficient mechanical stability of the resonators. An R&D program has been initiated

[19]The amplifier used for cw measurements delivers 1000 W. This corresponds to 300-500 Watts at the cavity

[20]The resolution of the eddy current system used at the moment allows to detect tantalum inclusions with a diameter of about 200 μm.

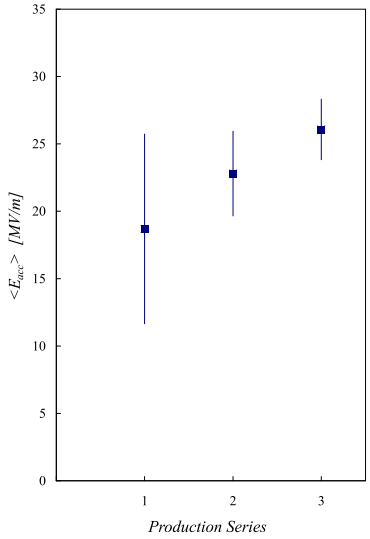

Figure 29: Average accelerating gradients at $Q_0 \geq 10^{10}$ of the cavities in the three TTF cavity productions measured in the vertical test cryostat. One can see the clear improvement due to tighter quality control of the sheet material and a tighter welding specification as well as improved handling in the clean-room environment.

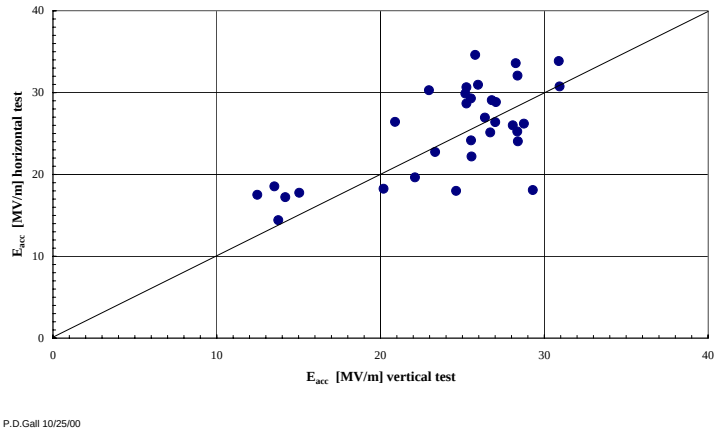

Figure 30: The distribution of the accelerating gradients in the acceptance test (vertical dewar) with the high power pulsed fullsystems test (horizontal cryostat or linac module).

aiming at improvements in all three directions. Furthermore, the feasibility of seamless cavities is being investigated.

3.4.1 Quality improvement of niobium

Niobium for microwave resonators has to be of high purity for several reasons: (a) dissolved gases like hydrogen, oxygen and nitrogen reduce the heat conductivity at liquid helium temperature and degrade the cooling of the rf surface; (b) contamination by foreign metals may lead to magnetic flux pinning and heat dissipation in rf fields; (c) normal-conducting or weakly superconducting clusters close to the rf surface are particularly dangerous . The Nb ingots contain about 500 ppm of finely dispersed tantalum. It appears unlikely that the Ta clusters found in some early TTF cavities might have been caused by this "natural" Ta content. Rather there is some suspicion that Ta grains might have dropped into the Nb melt during the various remeltings of the Nb ingot in an electron-beam melting furnace because such furnaces are often used for Ta production as well. To avoid contamination by foreign metals a dedicated electron-beam melting furnace would appear highly desirable but seems to be too cost-intensive in the present R&D phase of TESLA. Also more stringent requirements on the quality of the furnace vacuum (lower pressure, absence of hydrocarbons) would improve the Nb purity. The production steps following the EB melting (machining, forging and sheet rolling of the ingot) may also introduce dirt. The corresponding facilities need careful inspection and probably some upgrading. The present TTF cavities have been made from niobium with gas contents in the few ppm range and an RRR of 300. Ten 9-cell cavities have been measured both after 800°C and 1400°C firing. The average gain in gradient was about 4 MV/m. It would be highly desirable to eliminate the tedious and costly 1400°C heat treatment of complete cavities. One possibility might be to produce a niobium ingot with an RRR of more than 500. This is presently not our favored approach, mainly for cost reasons.

For the present R&D program, the main emphasis is on the production of ingots with $RRR \geq 300$, but with improved quality by starting from niobium raw material with reduced foreign material content, especially tantalum well below 500 ppm. Stricter quality assurance during machining, forging and sheet rolling should prevent metal flakes or other foreign material from being pressed into the niobium surface deeper than a few μm. To increase the RRR from 300 to about 600, it is planned to study the technical feasibility[21] of a

[21] At Cornell University cavities have been successfully fabricated from $RRR = 1000$ material. Likewise, the TTF cavity C19 was made from post-purified half cells and showed good performance.

1400°C heat treatment at the dumb-bell stage (2 half cells joined by a weld at the iris). This procedure would be preferable compared to the heat treatment of whole cavities which must be carefully supported in a Nb frame to prevent plastic deformation, while such a precaution is not needed for dumb-bells. However, there is a strong incentive to find cavity treatment methods which would permit elimination of the 1400°C heat treatment altogether. According to the results obtained at KEK [Saito et al. 1997] electropolishing seems to offer this chance (see below).

3.4.2 Improvement in cavity fabrication and preparation

Once half cells or dumb-bells of high RRR have been produced it is then mandatory to perform the electron-beam welding of the cavities in a vacuum of a few times 10^{-6} mbar in order to avoid degradation of the RRR in the welds. The EB welding machines available at industrial companies achieve vacua of only $5 \cdot 10^{-5}$ mbar and are hence inadequate for this purpose. An EB welding machine at CERN is equipped with a much better vacuum system. This EB apparatus is being used for a single-cell test program. For the future cavity improvement program a new electron-beam welding apparatus will be installed at DESY with a state-of-the-art electron gun, allowing computer-controlled beam manipulations, and with an oilfree vacuum chamber fulfilling UHV standards.

The industrially produced cavities undergo an elaborate treatment at TTF before they can be installed in the accelerator. A 150–200 μm thick damage layer is removed from the rf surface because otherwise gradients of 25 MV/m appear inaccessible. As explained in Sect. 3.2.3 the present method is Buffered Chemical Polishing (BCP) which leads to a rather rough surface with strong etching in the grain boundaries. An alternative method is "electropolishing" (EP) in which the material is removed in an acid mixture under current flow. Sharp edges and burrs are smoothed out and a very glossy surface can be obtained. For a number of years remarkable results have been obtained at KEK with electropolishing of 1-cell niobium cavities. Recently, a collaboration between KEK and Saclay has convincingly demonstrated that EP raises the accelerating field by more than 7 MV/m with respect to BCP. Several 1-cell cavities from Saclay, which showed already good performance after the standard BCP, exhibited a clear gain after the application of EP [Kako et al. 1999]. Conversely, an electropolished cavity which had reached 37 MV/m suffered a degradation after subsequent BCP. These results are a strong indication that electropolishing is the superior treatment method.

CERN, DESY, KEK and Saclay started a joint R&D program with electropolishing of half cells and 1-cell cavities in August 1998. Recent test results

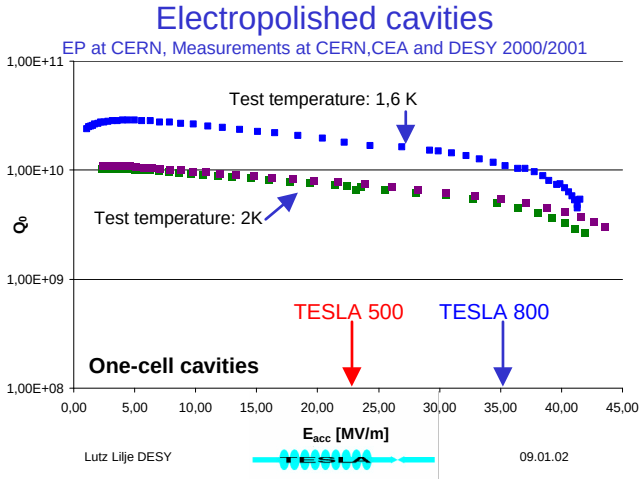

Figure 31: Examples of single-cell niobium cavities after electropolishing. The cavities show excellent performance over 40 MV/m.

yield gradients around 40 MV/m [Lilje et al. 1999] and hence the same good performance as was achieved at KEK. The transfer of the EP technology to 9-cell resonators requires considerable effort, although first tests in collaboration with KEK have resulted in a nine-cell cavity with an accelerating gradient of 32 MV/m in the cw measurement.

Recently it has been found [Lilje et al. 1999] that an essential prerequisite for achieving gradients in the 40 MV/m regime is a baking at 100 to 150°C for up to 48 hours while the cavity is evacuated, after the final high-pressure water rinsing. In electropolished cavities this procedure removes the drop of quality factor towards high gradients which is often observed without any indication of field emission. Such a drop is usually also found in chemically etched cavities; see for example Fig. 17. Experiments at Saclay [Visentin et al. 1998] have shown that a baking may improve the $Q(E)$ curve; however, part of the Q reduction at high field may be due to local magnetic field enhancements at the sharp grain boundaries of BCP treated cavities [Knobloch et al. 1999].

3.4.3 Mechanical stability of the cavities

The stiffening rings joining neighboring cells in the TESLA resonator are adequate to limit Lorentz-force detuning up to accelerating fields of 25 MV/m. Beyond 25 MV/m the cavity reinforcement provided by these rings is insuffi-

cient. Hence an alternative stiffening scheme must be developed for cavities in the 35–40 MV/m regime. A promising approach has been taken at Orsay and Saclay. The basic idea is to reinforce a thin-walled niobium cavity by a 2 mm thick copper layer which is plasma-sprayed onto the outer wall. Several successful tests have been made [Bousson 1999]. The copper plating has a potential danger since Nb and Cu have rather different thermal contraction. The deformation of a cavity upon cooldown and the resulting frequency shift need investigation. Another phenomenon has been observed in cavities made from explosion-bonded niobium-copper sheets: when these cavities were quenched, a reduction in quality factor Q_0 was observed. An explanation maybe trapped magnetic flux from thermo-electric currents at the copper-niobium interface. It is unknown whether this undesirable effect happens also in copper-sprayed cavities. An alternative to copper spraying might be the reinforcement of a niobium cavity by depositing some sort of metallic "foam", using the plasma or high velocity spraying technique. If the layer is porous the superfluid helium penetrating the voids should provide ample cooling.

The cavity reinforcement by plasma or high-velocity spraying appears to be a promising approach but considerable R&D work needs to be done to decide whether this is a viable technique for the TESLA cavities.

Alternatively the cavities can be actively tuned during the pulse using piezo-electric actuators. A successful demonstration of this scheme at TTF was performed. More detailed studies are underway.

3.4.4 The superstructure concept

The present TTF cavities are equipped with one main power coupler and two higher order mode couplers per 9-cell resonator. The length of the interconnection between two cavities has been set to $3\lambda/2$ ($\lambda = 0.23$ m is the rf wavelength) in order to suppress cavity-to-cavity coupling of the accelerating mode. A shortening of the interconnection is made possible by the "superstructure" concept, devised by J. Sekutowicz [Sekutowicz et al. 1999]. Four 7-cell cavities of TESLA geometry are joined by beam pipes of length ($\lambda/2$). The pipe diameter is increased to permit an energy flow from one cavity to the next, hence one main power coupler is sufficient to feed the entire superstructure. One HOM coupler per short beam pipe section provides sufficient damping of dangerous higher modes in both neighboring cavities. Each 7-cell cavity will be equipped with its own LHe vessel and frequency tuner. Therefore, in the superstructure the field homogeneity tuning (equal field amplitude in all cells) and the HOM damping can be handled at the sub-unit level. The main advantages of the superstructure are an increase

in the active acceleration length in TESLA - the design energy of 250 GeV per beam can be reached with a gradient of 22 MV/m - and a savings in rf components, especially power couplers.

A copper model of the superstructure is presently used to verify the theoretically predicted performance. This model allows individual cell tuning, field profile adjustment, investigation of transients in selected cells, test of the HOM damping scheme and measurement of the cavity couplings to the fundamental mode coupler. Also the influence of mechanical tolerances is studied. First results are promising [Sekutowicz et al. 1999]. A niobium superstructure prototype is under construction and will be tested with beam in the TTF linac beginning of 2001.

3.4.5 Seamless cavities

The EB welds in the present resonator design are a potential risk. Great care has to be taken to avoid holes, craters or contamination in the welds which usually have a detrimental effect on the high-field capability. A cavity without weld connections in the regions of high electric or magnetic rf field would certainly be less vulnerable to small mistakes during fabrication. For this reason the TESLA collaboration decided several years ago to investigate the feasibility of producing seamless cavities. Two routes have been followed: spinning and hydroforming.

At the Legnaro National Laboratory of INFN in Italy the spinning technique [Palmieri 1997a] has been successfully applied to form cavities out of niobium sheets. The next step will be to produce a larger quantity of 1-cell, 3-cell and finally 9-cell cavities from seamless Nb tubes with an RRR of 300. In the cavities spun from flat sheets a very high degree of material deformation was needed, leading to a rough inner cavity surface. Starting from a tube the amount of deformation will be much less and a smoother inner surface can be expected. Gradients up to 39 MV/m were obtained after electropolishing.

The hydroforming of cavities from seamless niobium tubes is being pursued at DESY [Gonin et al. 1999]. Despite initial hydroforming difficulties, related to inhomogeneous mechanical properties of the niobium tubes, four single cell cavities have been successfully built so far. In a recent test[22] 43 MV/m was achieved at $Q_0 = 1 \cdot 10^{10}$. The surface was prepared by electropolishing.

[22] Preparation and test of the hydroformed cavities were carried out by P. Kneisel at Jefferson Laboratory, Newport News, USA.

4 Auxiliary technical systems

4.1 Helium vessel and tuning system

The helium tank contains the superfluid helium needed for cooling and serves at the same time as a mechanical support of the cavity and as a part of the tuning mechanism. The tank is made from titanium whose differential thermal contraction relative to niobium is 20 times smaller than for stainless steel. Cooldown produces a stress of only 3 MPa in a cavity that was stress-free at room temperature. Titanium has the additional advantage that it can be directly electron-beam welded to niobium while stainless steel-niobium joints would require an intermediate metal layer.

The assembly of cavity and helium tank proceeds in the following sequence: a titanium bellows is electron-beam (EB) welded to the conical Nb head plate at one side of the cavity, a titanium ring is EB welded to the conical Nb head plate at other side. The cavity is then inserted into the tank and the bellows as well as the titanium ring are tungsten inert gas (TIG) welded to the Ti vessel.

The tuning system consists of a stepping motor with a gear box and a double lever arm. The moving parts operate at 2 K in vacuum. The tuning range is about ± 1 mm, corresponding to a frequency range of ± 300 kHz. The resolution is 1 Hz. The tuning system is adjusted in such a way that after cooldown the cavity is always under compressive force to avoid a backlash if the force changes from pushing to pulling.

4.2 Main Power Coupler

Design requirements

A critical component of a superconducting cavity is the power input coupler. For TTF several coaxial couplers have been developed [Brinkmann et al. 2001], consisting of a "cold part" which is mounted on the cavity in the clean room and closed by a ceramic window, and a "warm part" which is assembled after installation of the cavity in the cryomodule. The warm section contains the transition from waveguide to coaxial line. This part is evacuated and sealed against the air-filled wave guide by a second ceramic window. The elaborate two-window solution was chosen to get optimum protection of the cavity against contamination during mounting in the cryomodule and against window fracture during linac operation.

The couplers must allow for some longitudinal motion[23] inside the 12 m

[23] The motion of the coupler ports is up to 15 mm in the first cryomodules but has been

long cryomodule when the cavities are cooled down from room temperature to 2 K. For this reason bellows in the inner and outer conductors of the coaxial line are needed. Since the coupler connects the room-temperature waveguide with the 2 K cavity, a compromise must be found between a low thermal conductivity and a high electrical conductivity. This is achieved by several thermal intercepts and by using stainless steel pipes or bellows with a thin copper plating (10–20 μm) at the radio frequency surface. The design heat loads of 6 W at 70 K, 0.5 W at 4 K and 0.06 W at 2 K have been undercut in practice.

Electrical properties

An instantaneous power of 210 kW has to be transmitted to provide a gradient of 25 MV/m for an 800 μs long beam pulse of 8 mA. The filling time of the cavity amounts to 530 μs and the decay time, after the beam pulse is over, to an additional 500 μs. At the beginning of the filling, most of the rf wave is reflected leading to voltage enhancements by a factor of 2. The external quality factor of the coupler is $Q_{ext} = 3 \cdot 10^6$ at 25 MV/m. By moving the inner conductor of the coaxial line, Q_{ext} can be varied in the range $1 \cdot 10^6$ – $9 \cdot 10^6$ to allow not only for different beam loading conditions but also to facilitate an in-situ high power processing of the cavities. This feature has proved extremely useful on several occasions to eliminate field emitters that entered the cavities at the last assembly stage.

Input coupler A

The coupler version A is shown in Fig. 32. It has a conical ceramic window at 70 K and a commercial planar waveguide window at room temperature.

A conical shape was chosen for the cold ceramic window to obtain broadband impedance matching. The Hewlett-Packard High Frequency Structure Simulator program HFSS was used to model the window and to optimize the shape of the tapered inner conductor. The reflected power is below 1 %. The ceramic window is made from Al_2O_3 with a purity of 99.5%. Oxygen-free high-conductance copper rings are brazed to the ceramic using Au/Cu (35%/65%) braze alloy. The inner conductors on each side of the ceramic are electron-beam welded, the outer conductors are TIG welded. The ceramic is coated on both sides with a 10 nm titanium nitride layer to reduce multipacting.

reduced to about 1 mm in the most recent cryostat design by fixing the distance between neighboring cavities with invar rods.

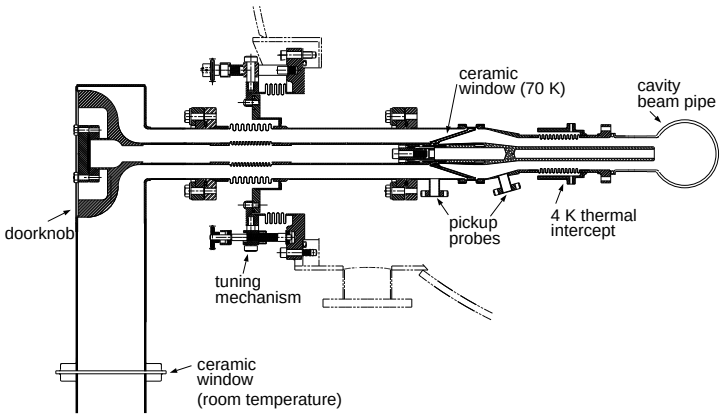

Figure 32: Simplified view of the power input coupler version A.

The waveguide-to-coaxial transition is realized using a cylindrical knob as the impedance-transforming device and a planar waveguide window. Matching posts are required on the air side of the window for impedance matching at 1.3 GHz.

Input couplers B, C

Coupler version B uses also a planar wave guide window and a door-knob transition from the wave guide to the coaxial line, but a cylindrical ceramic window at 70 K without direct view of the beam. Owing to a shortage in commercial wave guide windows a third type, C, was developed using a cylindrical window also at the wave guide - coaxial transition. It features a 60 mm diameter coaxial line with reduced sensitivity to multipacting and the possibility to apply a dc potential to the center conductor. In case of the LEP couplers [Tückmantel 1995] a dc bias has proved very beneficial in suppressing multipacting. Similar observations were made at DESY. All couplers needed some conditioning but have then performed according to specification.

4.3 Higher order modes

The intense electron bunches excite eigenmodes of higher frequency in the resonator which must be damped to avoid multibunch instabilities and beam breakup. This is accomplished by extracting the stored energy via higher-order mode (HOM) couplers mounted on the beam pipe sections of the nine-

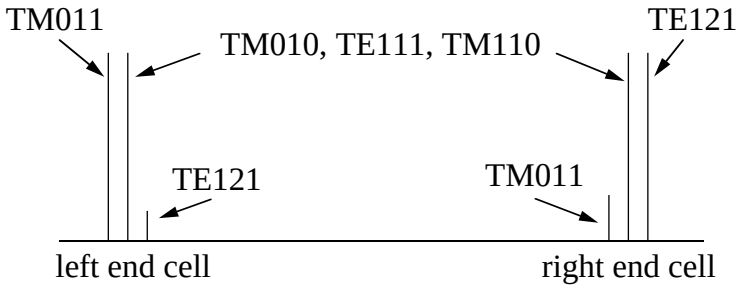

Figure 33: Effect of asymmetric end cell shaping on various modes. The main accelerating mode TM_{010} and the higher modes TE_{111} and TM_{110} are not affected while TM_{011} is enhanced in the left end cell, TE_{121} in the right end cell. Using HOM couplers at both ends, all higher order modes can be extracted.

cell resonator. A problem arises from "trapped modes" which are concentrated in the center cells and have a low field amplitude in the end cells. An example is the TE_{121} mode. By an asymmetric shaping of the end half cells one can enhance the field amplitude of the TE_{121} mode in one end cell while preserving the "field flatness" of the fundamental mode and also the good coupling of the HOM couplers to the untrapped modes TE_{111}, TM_{110} and TM_{011}. The effects of asymmetric end cell tuning are sketched in Fig. 33.

The two polarization states of dipole modes would in principle require two orthogonal HOM couplers at each side of the cavity. In a string of cavities, however, this complexity can be avoided since the task of the "orthogonal" HOM coupler can be taken over by the HOM coupler of the neighboring cavity. The viability of this idea was verified in measurements.

HOM coupler design

The HOM couplers are mounted at both ends of the cavity with a nearly perpendicular orientation[24] to ensure damping of dipole modes of either polarization. A 1.3 GHz notch filter is incorporated to prevent energy extraction from the accelerating mode. Two types of HOM couplers have been developed and tested, one mounted on a flange, the other welded to the cavity.

The demountable HOM coupler is shown in Fig. 34a. An antenna loop couples mainly to the magnetic field for TE modes and to the electric field for TM modes. The pickup antenna is capacitively coupled to an external load. The 1.3 GHz notch filter is formed by the inductance of the loop and the capacity at the 1.9 mm wide gap between loop and wall. A niobium bellows

[24]The angle between the two HOM couplers is not 90° but 115° to provide also damping of quadrupole modes.

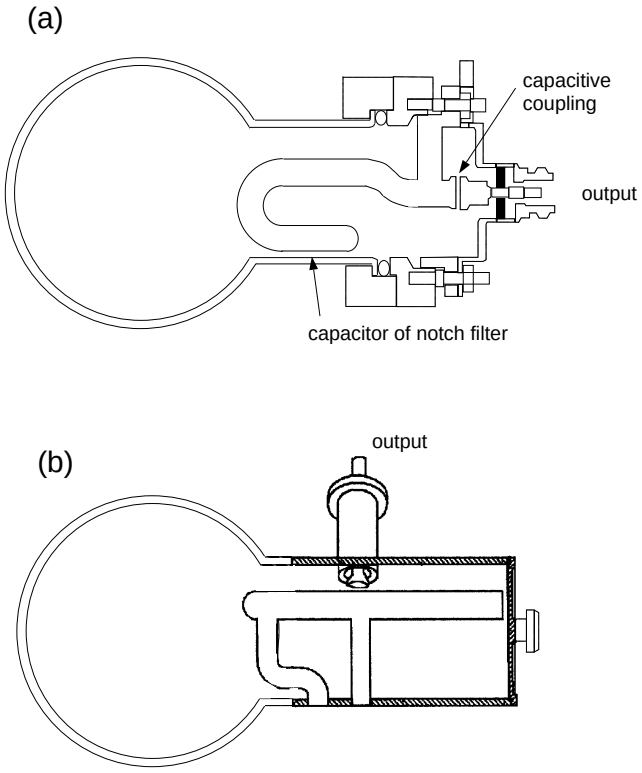

Figure 34: The higher-order-mode couplers: (a) demountable HOM coupler, (b) welded HOM coupler.

permits tuning of the filter without opening the cavity vacuum. The antenna is thermally connected to the 2 K helium bath. In a cw (continuous wave) test at an accelerating field of 21 MV/m the antenna reached a maximum temperature of 4 K, which is totally uncritical.

The welded version of the HOM coupler is shown in Fig. 34b. It resembles the couplers used in the 500 MHz HERA cavities which have been operating for several years without quenches. The good cooling of the superconducting inner conductor by two stubs makes the design insensitive to γ radiation and electron bombardment.

Both HOM couplers permit tuning of the fundamental mode rejection filter when mounted on the cavity. It is possible to achieve a Q_{ext} of more than 10^{11} thereby limiting power extraction to less than 50 mW at 25 MV/m.

4.4 RF Control System and Performance of the Cavities with Electron Beam

4.4.1 General demands on the rf control system

The requirements on the stability of the accelerating field in a superconducting acceleration structure are comparable to those in a normal-conducting cavity. However the nature and magnitude of the perturbations to be controlled are rather different. Superconducting cavities possess a very narrow bandwidth and are therefore highly susceptible to mechanical perturbations. Significant phase and amplitude errors are induced by the resulting frequency variations. Perturbations can be excited by mechanical vibrations (microphonics), changes in helium pressure and level, or Lorentz forces. Slow changes in frequency, on the time scale of minutes or longer, are corrected by a frequency tuner, while faster changes are counteracted by an amplitude and phase modulation of the incident rf power.

The demands on amplitude and phase stability of the TESLA Test Facility cavities are driven by the maximum tolerable energy spread in the TTF linac. The design goal is a relative spread of $\sigma_E/E = 2 \cdot 10^{-3}$ implying a gradient and phase stability in the order of $1 \cdot 10^{-3}$ and 1.6°, respectively. For cost reasons up to 32 cavities will be powered by a single klystron. Hence it is not possible to control individual cavities but only the vector sum of the field vectors in these 32 cavities.

One constraint to be observed is that the rf power needed for control should be minimized. The rf control system must also be robust against variations of system parameters such as beam loading and klystron gain.

The pulsed structure of the rf power and the beam at TTF, shown in Fig. 35, puts demanding requirements on the rf control system. Amplitude and phase control is obviously needed during the flat-top of 800 μs when the beam is accelerated, but it is equally desirable to control the field during cavity filling to ensure proper beam injection conditions. Field control is aggravated by the transients induced by the subpicosecond electron bunches which have a repetition rate of 1 to 9 MHz.

For a detailed discussion of the basic principles of rf systems used in superconducting electron linacs and their operational performance, refer to [Gräf 1995] and [Simrock 1993].

4.4.2 Sources of field perturbations

There are two basic mechanisms which influence the magnitude and phase of the accelerating field in a superconducting cavity:

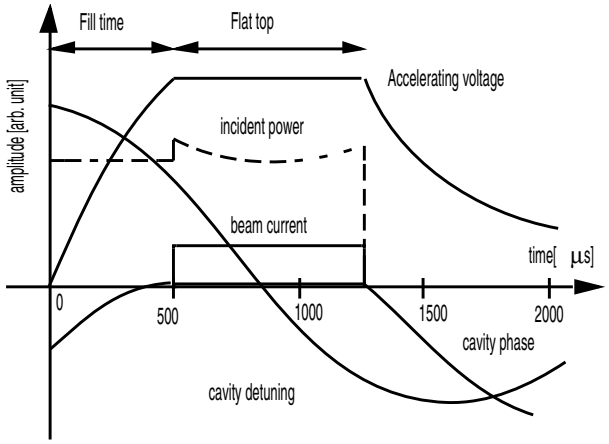

Figure 35: Pulse structure of TTF cavity operation. Shown are: accelerating voltage with 500 μs filling time and 800 μs flat top, incident power, beam current, cavity phase and cavity detuning.

- variations in klystron power or beam loading (bunch charge)
- modulation of the cavity resonance frequency.

Perturbations of the accelerating field through time-varying field excitations are dominated by changes in beam loading. One must distinguish between transients caused by the pulsed structure of the beam current and stochastic fluctuations of the bunch charge. The transients caused by the regular bunch train in the TTF linac (800 sub-picosecond bunches of 8 nC each, spaced by 1 μs) are in the order of 1% per 10 μs; the typical bunch charge fluctuations of 10% induce field fluctuations of about 1%. In both cases the effect of the fast source fluctuations on the cavity field is diminuished by the long time constant of the cavity[25].

Mechanical changes of the shape and eigenfrequency of the cavities caused by microphonics are a source of amplitude and phase jitter which has bothered superconducting accelerator technology throughout its development. In the TTF cavities the sensitivity of the resonance frequency to a longitudinal deformation is about 300 Hz/μm. Heavy machinery can transmit vibrations through the ground, the support and the cryostat to the cavity. Vacuum pumps can interact with the cavity through the beam tubes, and the compressors and pumps of the refrigerator may generate mechanical vibrations

[25]The cavity with power coupler is adjusted to an external Q of $3 \cdot 10^6$ at 25 MV/m, corresponding to a time constant of about 700 μs. The consequence is a low-pass filter characteristic.

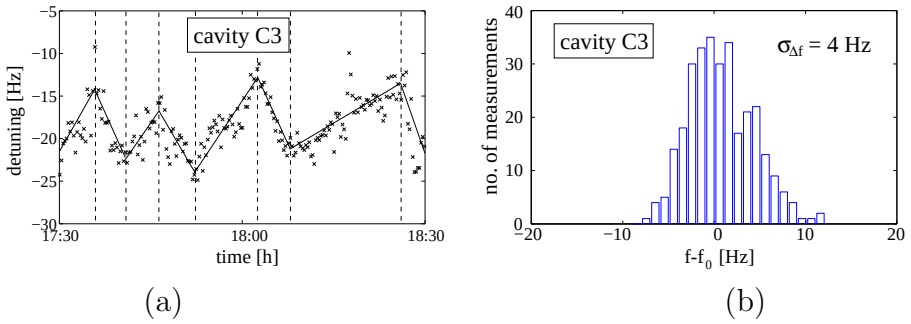

(a) (b)

Figure 36: Fluctuations of the cavity resonance frequency. (a) Slow drifts caused by helium pressure variations. The sensitivity is 10 Hz/mbar. (b) Random variations of resonance frequency after correction for the slow drift.

which travel along the He transfer line into the cryostat. Also helium pressure variations lead to changes in resonance frequency as shown in Fig. 36a. The rms frequency spread due to microphonics, measured in 16 cavities, is 9.5 ± 5.3 Hz and thus surprisingly small for a superconducting cavity system (see Fig. 36b).

At high accelerating gradients the Lorentz forces become a severe perturbation. The corresponding frequency shift is proportional to the square of the accelerating field according to $\Delta f = -K \cdot E_{\mathrm{acc}}^2$ with $K \approx 1$ Hz/(MV/m)^2. Figure 37a shows a cw measurement of the resonance curve with a strong distortion caused by Lorentz forces. In cw operation the frequency shift can be easily corrected for by mechanical tuning. In the pulsed mode employed at the TTF linac this is not possible since the mechanical tuner is far too slow. Hence a time-dependent detuning is unavoidable. In order to keep the deviation from the nominal resonance frequency within acceptable limits the cavities are predetuned before filling. The measured dynamic detuning of cavity C39 during the 1.3 ms long rf pulse is shown in Fig. 37b for accelerating fields of 15 to 30 MV/m. Choosing a predetuning of +300 Hz, the eigenfrequency at 25 MV/m changes dynamically from +100 Hz to −120 Hz during the 800 μs duration of the beam pulse.

In steady state (cw) operation at a gradient of 25 MV/m and a beam current of 8 mA a klystron power of 210 kW is required per nine-cell cavity. In pulsed mode $\approx$ 15 % additional rf power is needed to maintain a constant accelerating gradient in the presence of cavity detuning. The frequency changes from microphonics and helium pressure fluctuations lead to comparable extra power requirements. The klystron should be operated 10 % below saturation to guarantee sufficient gain in the feedback loop.

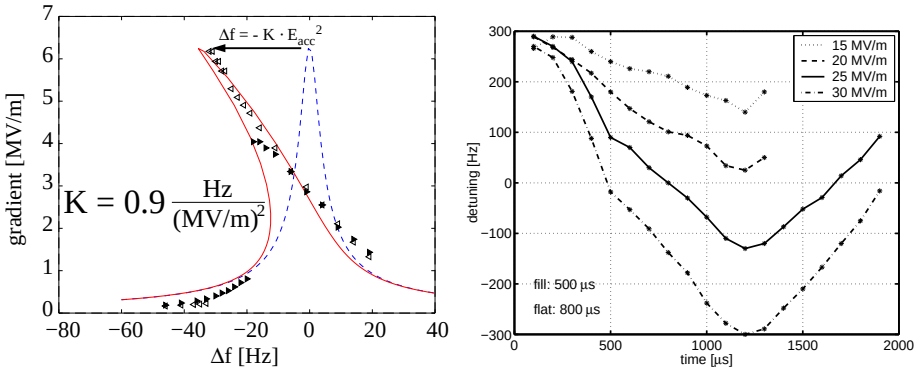

Figure 37: (Left) Influence of Lorentz forces on the shape of the resonance curve of a sc cavity in cw operation. The left part of the curve was mapped out by approaching the resonance from below, the right part by coming from above. (Right) Dynamical detuning of cavity C39 during the TESLA pulse. In pulsed operation the resonance is approached from above.

4.4.3 RF control design considerations

The amplitude and phase errors from Lorentz force detuning, beam transients and microphonics are in the order of 5% and 20°, respectively. These errors must be suppressed by one to two orders of magnitude. Fortunately, the dominant errors are repetitive (Lorentz forces and beam transients) and can be largely eliminated by means of a feedforward compensation. It should be noted, however, that bunch-to-bunch fluctuations of the beam current cannot be suppressed by the rf control system since the gain bandwidth product is limited to about 1 MHz due to the low-pass characteristics of the cavity, the bandwidth limitations of electronics and klystrons, and cable delay.

Fast amplitude and phase control can be accomplished by modulation of the incident rf wave which is common to 32 cavities. The control of an individual cavity field is not possible. The layout of the TTF digital rf control system is shown in Fig. 38. The vector modulator for the incident wave is designed as a so-called "I/Q modulator" controlling real and imaginary part of the complex cavity field vector instead of amplitude and phase. This has the advantage that the coupling between the two feedback loops is minimized and the problem of large phase uncertainties at small amplitude is avoided.

The detectors for cavity field, incident and reflected wave are implemented as digital detectors for real and imaginary part. The rf signals are converted to an intermediate frequency of 250 kHz and sampled at a rate of 1 MHz, which means that two subsequent data points yield the real and the imaginary part of the cavity field vectors. These vectors are multiplied with 2×2 rota-

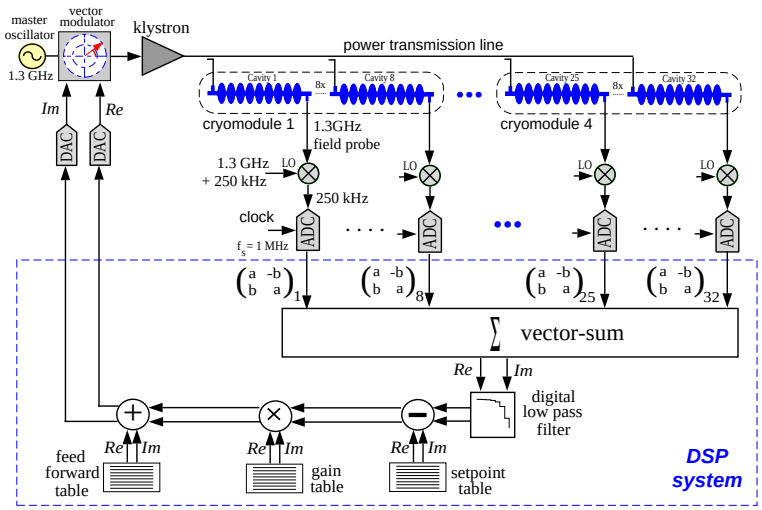

Figure 38: Schematic of the digital rf control system.

tion matrices to correct for phase offsets and to calibrate the gradients of the individual cavity probe signals. The vector sum is calculated and a Kalman filter is applied which provides an optimal state (cavity field) estimate by correcting for delays in the feedback loop and by taking stochastic sensor and process noise into account. Finally the nominal set point is subtracted and a time-optimal gain matrix is applied to calculate the new actuator setting (the *Re* and *Im* control inputs to the vector modulator). Adaptive feedforward is realized by means of a table containing the systematic variations, thereby reducing the task of the feedback loop to control the remaining stochastic fluctuations. The feedforward tables are continuously updated to take care of slow changes in parameters such as average detuning angle, microphonic noise level and phase shift in the feedforward path.

4.4.4 Operational experience

The major purpose of the TESLA Test Facility linac is to demonstrate that all major accelerator subsystems meet the technical and operational requirements of the TESLA collider. Currently the TTF linac is equipped with two cryomodules each containing 8 cavities. The cavities are routinely operated at the design gradient of TTF of 15 MV/m, providing a beam energy of 260 MeV. The 2 modules can perform at a maximum average gradient of 20 and 22 MV/m respectivly.

An important prerequisite of the proper functioning of the vector-sum control of 16 to 32 cavities is an equal response of the field pickup probes

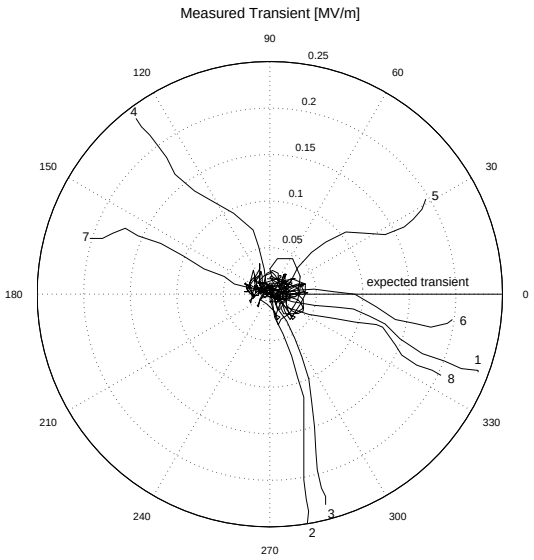

Figure 39: Beam induced transients (cavity field vectors) obtained by measuring the cavity fields with and without beam pulses. The noise in the signals can be estimated from the erratic motion at the center of the plot. This region represents the first 50 μs of the measurement before the arrival of the beam pulse.

in the individual cavities. A first step is to adjust the phase of the incident rf wave to the same value in all cavities by means of three-stub tuners in the wave guides. Secondly, the transients induced by the bunched beam are used to obtain a relative calibration of the pickup probes, both in terms of amplitude and phase. Typical data taken at the initial start-up of a linac run are shown in Fig. 39. Ideally the lengths of the field vectors should all be identical since the signals are induced by the same electron bunch in all cavities. The observed length differences indicate a variation in the coupling of the pickup antenna to the beam-induced cavity field, which has to be corrected. The different phase angles of the field vectors are mainly due to different signal delays. The complex field vectors are rotated by matrix multiplication in digital signal processors to yield all zero phase. Moreover they are normalized to the same amplitude to correct for the different couplings of the pickup antennas to the cavity fields. Once this calibration has been performed the vector sum of the 16 or 32 cavities is a meaningful measure of the total accelerating voltage supplied to the beam. The calibration is verified with a measurement of the beam energy in a magnetic spectrometer.

The required amplitude stability of $1{\cdot}10^{-3}$ and phase stability of $\sigma_\phi \leq 1.6^\circ$ can be achieved during most of the beam pulse duration with the exception

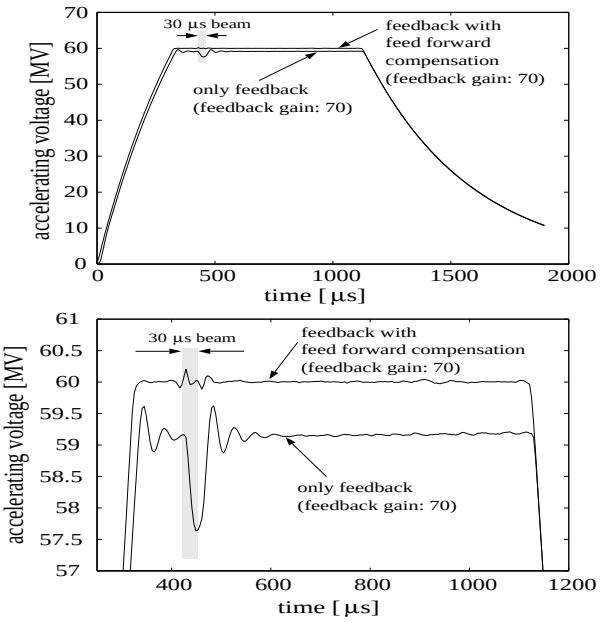

Figure 40: Field regulation of the vector-sum of 8 cavities without and with adaptive feedforward. The lower graph shows an enlarged view of the plateau region.

of the beam transient induced when turning on the beam. Without feedback the transient of a 30 μs beam pulse at 8 mA would be of the order of 1 MV/m. This transient can be reduced to about 0.2 MV/m by turning on feedback. The effectiveness of the feedback system is limited by the loop delay of 5 μs and the unity-gain bandwidth of about 20 kHz. The 0.2 MV/m transient is repetitive with a high degree of reproducibility. Using feedforward it can be further suppressed by more than an order of magnitude, as shown in Fig. 40. Slow drifts are corrected for by making the feedforward system adaptive [Liepe and Simrock 1998]. The feedforward tables are updated on a time scale of minutes.

References

[Albach and Voss 1957]
W. Albach and G. Voss, Zeitschr. Angew. Phys, **9**:111, 1957. 47

[Aune et al. 2000]
B. Aune et al., The Superconducting TESLA Cavities, PRST-AB, **3**, September 2000, 092001. 6, 39, 54

[Bahte et al. 1997]
M. Bahte, F. Herrmann, and P. Schmüser, Magnetization and Susceptibility Measurements on Niobium Samples for Cavity Production, In *Proceedings of the 8th Workshop on RF Superconductivity* [Palmieri 1997b]. 24

[Bahte 1998]
M. Bahte, Materialuntersuchungen an supraleitenden Niob-Proben mit Magnetisierungs- und Suszeptibilitätsmessungen, Diplomarbeit, Universität Hamburg, 1998, DESY FDET-98-01. 23, 24, 85

[Bardeen et al. 1957]
J. Bardeen, L. Cooper, and J. R. Schrieffer, Theory of Superconductivity, Physical Review, **108**:1175, 1957. 21

[Bernard et al. 1992]
P. Bernard et al., LEP cavities, in *Proceedings of the 1992 European Particle Accelerator Conference*, edited by E. H. *et al.*, p. 1269, Editions Frontieres, 1992. 53

[Bonin et al. 1992]
B. Bonin, H. Safa, J. Charrier, et al., Flux trapping in superconducting cavities, in *Proceedings of the 3rd EPAC*, p. 1295, 1992. 28

[Bonin 1995]
P. Bonin, editor, *Proceedings of the 7th Workshop on RF Superconductivity*, volume I+II, Gif-sur-Yvette, October 1995, IN2P3. 74, 79

[Bonin 1996a]
B. Bonin, Supercond. Sci. Technology, **9**:453, 1996. 32, 82

[Bonin 1996b]
B. Bonin, Materials for superconducting cavities, in *Superconductivity in Particle Accelerators*, edited by S. Turner, pp. 191–200, CERN, May 1996, CERN 96-03. 27, 32

[Boucheffa et al. 1995]
A. Boucheffa et al., Kapitza conductance of niobium for superconducting cavities in the temperature range 1,6 , 2 K, In *Proceedings of the 7th Workshop on RF Superconductivity* [Bonin 1995], p. 659. 52

[Bousson 1999]
S. Bousson, in *Proceedings of the 9th Workshop on RF Superconductivity*, 1999. 60

[Brinkmann et al. 2001]
R. Brinkmann, K. Flöttmann, J. Rossbach, P. Schmüser, N. Walker, and H. Weise, editors, *TESLA - Technical Design Report*, volume II, DESY, March 2001, DESY 2001 - 011, ECFA 2001-209, TESLA Report 2001-23. 5, 41, 53, 54, 62, 83, 85

[Brinkmann et al. 1997]
R. Brinkmann, G. Materlik, J. Rossbach, and A. Wagner, editors, *Conceptual Design Report of a 500 GeV e+e- Linear Collider with Integrated X-ray Laser Facility*, volume I+II, DESY, 1997, DESY 97-048. 5

[Budliger and Laisne 1968]
J. Budliger and A. Laisne, Effet d'Avalanche en Geometrie Plane et Cylindrique, Nuclear Instruments and Methods, **61**:253, 1968. 37

[Doll and Graf 1967]
R. Doll and P. Graf, Superheating in Cylinders of Pure Superconducting Tin, Phys. Rev. Lett., **19**:897, 1967. 24

[Farnsworth 1934]
P. T. Farnsworth, Multiple Impacting Electron Amplifier, J. Franklin Inst., **218**:411, 1934, nach A. J. Hatch 1966. 37

[Fouaidy et al. 1992]
M. Fouaidy, T. Junquera, and A. Caruette, Surface Temperature Measurements on Superfluid Helium, in *Proceedings of the 5th Workshop on RF Superconductivity*, edited by D. Proch, volume I+II, Hamburg, April 1992, DESY, DESY-M-92-01. 30

[Fuss 1976]
J. Fuss, Diplomarbeit, Universität Stuttgart, 1976. 31

[Gonin et al. 1999]
I. Gonin et al., in *Proceedings of the 9th Workshop on RF Superconductivity*, 1999. 61

[Graber et al. 1994]
J. Graber et al., Reduction of field emission in superconducting cavities with high pulsed power RF, Nucl. Instrum. and Methods A, **350**:572, 1994. 53

[Graber 1993]
J. Graber, High Power RF Processing Studies of 3 GHz Niobium Superconducting Accelerator Cavites, PhD thesis, Cornell University, 1993. 35

[Gräf 1995]
H.-D. Gräf, in *Proceedings of the 5th Workshop on RF Superconductivity*, number DESY M-92-01, p. 317, 1995. 67

[Halbritter 1970]
J. Halbritter, Calculation of the BCS surface resistance, Z. f. Phys., **238**:466, 1970. 27, 28

[Hatch and Williams 1954]
A. Hatch and H. Williams, The secondary electron resonance mechanism of low-pressure High-frequency gas breakdown, J. o. Appl. Phys., **25**:417, April 1954. 37

[Hays and Padamsee 1997]
T. Hays and H. Padamsee, Measuring the RF critical field of Pb, Nb and Nb_3Sn, In *Proceedings of the 8th Workshop on RF Superconductivity* [Palmieri 1997b], p. 789. 24, 55

[Hörmann 1986]
M. Hörmann, Erstellung von hochwärmeleitfähigem Niob im technischen Massstab für die Hochfrequenzsupraleitung, Z. f. Metallkunde, **77**:338, 1986. 31, 85

[Kako et al. 1999]
E. Kako et al., Improvement Of Cavity Performance In The Saclay/Cornell/Desy's Sc Cavities, In *Proceedings of the 9th Workshop on RF Superconductivity* [Krawcyk 1999], TUP011. 58

[Kneisel 1999]
P. Kneisel, Preliminary experience with "in-situ" baking of niobium cavities, In *Proceedings of the 9th Workshop on RF Superconductivity* [Krawcyk 1999]. 36

[Knobloch et al. 1997]
J. Knobloch, W. Hartung, H. Padamsee, and F. Newman, Multipacting in 1,5 GHz superconducting niobium cavities of the CEBAF shape, In *Proceedings of the 8th Workshop on RF Superconductivity* [Palmieri 1997b], p. 1017. 38

[Knobloch et al. 1999]
J. Knobloch, M. Liepe, R. Geng, and H. Padamsee, High-Field Q slope in Superconducting Cavities Due to Magnetic Field Enhancement at Grain Boundaries, In *Proceedings of the 9th Workshop on RF Superconductivity* [Krawcyk 1999], pp. 77–91. 59

[Knobloch 1997]
J. Knobloch, Advanced Thermometry Studies of Superconducting RF Cavities, PhD thesis, Cornell University, August 1997, CLNS Thesis 97-3. 29, 35, 38

[Krawcyk 1999]
F. Krawcyk, editor, *Proceedings of the 9th Workshop on RF Superconductivity*, volume I+II, Santa Fe, November 1999, LANL. 76, 77, 80, 81

[Lauströer et al. 1987]
U. Lauströer et al., URMEL and URMEL-T USER GUIDE (Mode Analysis of Cylindrically Symmetric Cavities; Evaluation of RF-Fields in Waveguides), Technical Report DESY M-87-03, DESY, 1987. 45

[Liepe and Simrock 1998]
M. Liepe and S. Simrock, in *Proceedings EPAC 1998*, edited by S. Myers, L. Liljeby, C. Petit-Jean-Genaz, J. Poole, and K.-G. Rensfelt, p. 1735, 1998, Stockholm, Sweden. 73

[Lilje et al. 1999]
L. Lilje et al., Electropolishing and in-situ Baking of 1.3 GHz Niobium Cavities, In *Proceedings of the 9th Workshop on RF Superconductivity* [Krawcyk 1999]. 36, 59

[Matricon and Saint-James 1967]
J. Matricon and D. Saint-James, Superheating fields in superconductors, Phys. Lett., **24A**:241, 1967. 24, 25

[Mittag 1973]
K. Mittag, Kapitza conductance and thermal conductivity of copper, niobium and aluminium in the range from 1.3 to 2.1 K, Cryogenics, p. 94, 1973. 30, 33

[Müller 1988a]
G. Müller, in *Proceedings of the 3rd Workshop on RF Superconductivity*, p. 331, 1988. 32, 48, 82

[Müller 1988b]
G. Müller, Superconducting Niobium in High RF Magnetic Fields, In *Proceedings of the 3th Workshop on RF Superconductivity* [Shepard 1988], pp. 331–358, ANL-PHY-88-1. 53

[Padamsee et al. 1990]
H. Padamsee et al., Superconducting RF activities at Cornell University, in *Proceedings of the 4th Workshop on RF Superconductivity*, edited by Y. Kojima, volume I+II, Tsukuba, 1990, KEK, KEK Report 89-21. 53

[Padamsee et al. 1998]
H. Padamsee, J. Knobloch, and T. Hays, *RF Superconductivity for Accelerators*, John Wiley & Sons, 1998. 6, 23, 29, 32, 44, 85

[Padamsee 1990]
H. Padamsee, editor, *Proceedings of the 1st TESLA WORKSHOP*, Cornell University, 1990, CLNS-90-1029. 38

[Padamsee 2001]
H. Padamsee, The science and technology of superconducting cavities for particle accelerators, Supercond. Sci. Tech., **14**:R28, 2001. 6, 39

[Palmer 1988]
F. Palmer, Surface resistance of Superconductors - Examples from Nb - O system, In *Proceedings of the 3th Workshop on RF Superconductivity* [Shepard 1988], p. 309, ANL-PHY-88-1. 28

[Palmieri 1997a]
V. Palmieri, in *Proceedings of the 8th Workshop on RF Superconductivity*, edited by V. Palmieri and A. Lombardi, p. 553, 1997, Abano Terme, Italy. 61

[Palmieri 1997b]
V. Palmieri, editor, *Proceedings of the 8th Workshop on RF Superconductivity*, volume I+II, Abano terme, October 1997, INFN. 74, 76, 79

[Pekeler et al. 1995]
M. Pekeler et al., An advanced rotating T-R mapping and its diagnosis of TESLA 9-cell superconducting cavity, in *Proceedings of the Particle Accelerator Conference and International Conference on High Energy Accelerators*, p. 1639, 1995. 29

[Pekeler 1996]
M. Pekeler, Untersuchungen der feldbegrenzenden Mechanismen in supraleitenden Niob-Resonatoren, PhD thesis, Universität Hamburg, August 1996, DESY M 96-16. 30

[Piel 1989]
H. Piel, Superconducting cavities, in *Superconductivity in Particle Accelerators*, edited by S. Turner, p. 149, CERN, May 1989, CERN 89-04. 24, 39

[Piosczyk 1974]
B. Piosczyk, Exerimentelle Untersuchungen an supraleitenden Wendelresonatoren aus Niob im 100 MHz-Bereich, PhD thesis, Universität Karlsruhe, 1974, KFK 1991. 28

[Pippard 1953]
A. B. Pippard, Impurities in superconductors, Proc . Roy. Soc (London), **A203**:98, 1953. 23

[Reece et al. 1995]
C. Reece et al., Performance experience with the CEBAF SRF cavities, in *Proceedings of the Particle Accelerator Conference and International Conference on High Energy Accelerators*, p. 1512, 1995. 35, 39

[Reschke 1995]
D. Reschke, Untersuchungen an 3GHz Niobresonatoren, PhD thesis, Universität Wuppertal, 1995, WUP-DIS 95-5. 28, 35

[Reschke 1997]
D. Reschke, Thermal model calculations for 1,3 GHz TTF accelerator cavities, In *Proceedings of the 8th Workshop on RF Superconductivity* [Palmieri 1997b], p. 385. 33

[Reschke 2001]
D. Reschke, Thermal simulations on high RRR niobium, Private communication, 2001. 34

[Safa et al. 1995]
H. Safa et al., Nb purification by Ti gettering, In *Proceedings of the 7th Workshop on RF Superconductivity* [Bonin 1995], p. 649. 53

[Saito and Kneisel 1999]
K. Saito and P. Kneisel, Temperature Dependence of the Surface Resistance of Niobium at 1300 MHz - Comparison to BCS Theory -, In *Proceedings of the 9th Workshop on RF Superconductivity* [Krawcyk 1999]. 27, 28

[Saito et al. 1997]
K. Saito et al., High accelerating gradients in niobium L-Band cavities, Particle Accelerators, **60**:193, 1997. 58

[Schilcher 1995]
T. Schilcher, Wärmeleitvermögen von Niob bei kryogenischen Temperaturen, Diplomarbeit, Universität Regensburg, 1995, TESLA 95-12. 32, 33, 82

[Schulze 1981]
K. K. Schulze, Preparation and Characterization of Ultra-High-Purity niobium, J. Metals, **33**:33, May 1981. 31

[Sciver 1986]
S. Sciver, *Helium Cryogenics*, Plenum Press, 1986. 29

[Sekutowicz et al. 1999]
J. Sekutowicz, M. Ferrario, and C. Tang, Phys. Rev. ST Accel. Beams, **2**, 1999. 60, 61

[Shepard 1988]
K. Shepard, editor, *Proceedings of the 3th Workshop on RF Superconductivity*, volume I+II, Argonne, 1988, ANL, ANL-PHY-88-1. 78

[Silari et al. 1999]
M. Silari, S. Agosteo, J.-C. Gaborit, and L. Ulrici, Radiation produced by the LEP superconducting cavities, Nuclear Instruments and Methods A, **432**:1 , 1999. 35

[Simrock 1993]
S. Simrock, in *Proceedings of the 6th Workshop on RF Superconductivity*, edited by R. M. Sundelin, p. 294, 1993. 67

[Stolzenburg 1996]
C. Stolzenburg, Untersuchung zur Entstehung von Dunkelstrom in supraleitenden Beschleunigungsstrukturen, PhD thesis, Universität Hamburg, Mai 1996. 36

[Tückmantel 1995]
J. Tückmantel, p. 1642, 1995. 64

[Visentin et al. 1998]
B. Visentin, J. Charrier, and B. Coadou, Improvements of superconducting cavity performances at high gradients, in *Proceedings of the 6th EPAC*, volume III, p. 1885, 1998. 36, 59

[Visentin et al. 1999]
B. Visentin, J. Charrier, B. Coadou, and D. Roudier, Cavity baking: A cure for the high accelerator field Q_0 drop, In *Proceedings of the 9th Workshop on RF Superconductivity* [Krawcyk 1999]. 36

[Waldram 1964]
J. Waldram, Surface Impedance of Superconductors, Adv. Phys., **13**:1, 1964. 23

[Weingarten et al. 1984]
W. Weingarten et al., Electron loading, in *Proceedings of the 2th Workshop on RF Superconductivity*, edited by H. Lengeler, volume I+II, p. 573, Genf, 1984, CERN. 37

[Weingarten 1995]
W. Weingarten, in *CERN Accelerator School "Superconductivity in Particle Accelerators"*, number CERN 96-03, p. 167, CERN, Hamburg, 1995. 27

[Yogi et al. 1977]
T. Yogi, G. Dick, and J. E. Mercereau, Critical rf Magnetic Fields for some Type-I and Type-II Superconductors, Phys. Rev. Lett., **39**:826, 1977. 25

List of Figures

List of Tables